# Comparison of core-hole excitation spectra of organic donor/acceptor molecules in the vapor and condensed phases: p-Nitroaniline, 2-amino-6-nitronaphthalene and 1-amino-4-nitronaphthalene

H.-J. Freund[a]

*Institut für Physikalische und Theoretische Chemie, Universität Erlangen-Nürnberg, Egerlandstrasse 3, 8520 Erlangen, West Germany*

A. R. Slaughter, S. M. Ballina, and M. S. Banna

*Department of Chemistry, Vanderbilt University, Nashville, Tennessee 37235*

R. W. Bigelow

*Xerox Webster Research Center, Webster, New York 14580*

B. Dick, J. Lex

*Institut für Organische Chemie, Universität zu Köln, Greinstr. 4, 5000 Köln 41, West Germany*

H. M. Deger

*Hoechst AG, Hauptlaboratorium, 6230 Frankfurt/Main 80, West Germany*

Vapor phase $N1s$ and $O1s$ core-hole spectra of the organic donor/acceptor molecules 2-amino-6-nitronaphthalene (2,6-ANN) and 1-amino-4-nitronaphthalene (1,4-ANN) are presented and compared to condensed phase results. 2,6-ANN and 1,4-ANN are found to exhibit broad single peak $N1s(NO_2)$ signals in the gas phase which become split into resolvable components in the solid. The spectral differences noted on going from the vapor phase to the solid parallel previous results on p-nitroaniline (PNA). Unlike the situation encountered in PNA (and 2,6-ANN), however, the $O1s(NO_2)$ spectrum of 1,4-ANN also indicates a moderately increased splitting as well as an apparent decrease in shake-up intensity on going from the vapor to the condensed phase. Spectral differences between the two phases are addressed within the CNDO/S(CI) equivalent-core approximation including up to doubly excited "singlet-coupled" configurations as a means of elucidating the apparent core-hole induced intermolecular coupling. Comparison computations are presented on PNA, 2,6-ANN, and 1,4-ANN. X-ray crystallographic measurements on 2,6-ANN indicate an intermolecular donor/acceptor pairing scheme as in PNA. Dimer models are therefore used to computationally address solid state interactions. The $N1s(NO_2)$ spectral differences observed in PNA, 2,6-ANN, and 1,4-ANN on going from the vapor to the condensed phase are attributed to strong core-hole induced intermolecular orbital mixing. Explicit inclusion of doubly excited configurations in both the monomer and dimer (solid) computations is essential to achieve theoretical assignments of the $N1s(NO_2)$ and $O1s(NO_2)$ spectra consistent with experiment. The results are analyzed in terms of dominant single and doubly excited contributions.

## INTRODUCTION

There has recently been considerable interest in the origin of the intense multipeak structure observed in the core-hole spectra of organic donor/acceptor molecules $(D^+-Ar-A^-)$.[1–30] Numerous studies, primarily describing the results of condensed phase measurements, have attributed such structure to shake-up processes arising from the concomitant creation of a core-hole and *intramolecular* $\pi^* \leftarrow \pi$ charge-transfer excitation(s). Several explicit molecular orbital studies on p-nitroaniline (PNA) and related molecules appear to verify the shake-up interpretation as opposed to extrinsic processes such as radiation damage or hydrogen bonding effects.[7–9,13–17] Essentially, creation of a positively charged core-hole on the acceptor group [the $N1s(NO_2)$

core-hole in the case of PNA, for example] dramatically reduces the separation between the highest occupied donor orbital and lowest unoccupied acceptor level due to selective Coulomb interactions leading to low energy satellite structure. The satellite intensity is determined by the details of the hole screening mechanism which can be addressed with reference to the one-electron states of the neutral system in terms of hole-induced orbital mixing of occupied and unoccupied levels.[31–33]

Of particular interest to us is the recent observations that certain $D^+-Ar-A^-$ systems exhibit vapor phase core-hole spectra considerably different from that found for the solid state.[12,28] The first example of such *solid state effects* were noted for PNA (Fig. 1).[12] Briefly, PNA was initially found to exhibit a well-resolved doublet peak $N1s(NO_2)$ spectrum in the solid $(\Delta E \sim 1.8$ eV) with approximately equal intensity components.[1,2] PNA in the gas phase, how-

ever, was shown to yield a broad single peak $N1s(NO_2)$ spectrum which, upon greater resolution, was subsequently shown to consist of an asymmetric peak structure with approximately 30% of the total intensity appearing as a low-lying satellite on the high binding energy side of the main line $(\Delta E \sim 1.25 \text{ eV})$.[25] Although numerous comparisons between condensed phase core-hole spectra of $D^+-Ar-A^-$ systems and molecular orbital computations on the isolated molecular species using singly excited configurations have indicated some striking correlations, the results on PNA suggest that such parallels may, in some cases, be misleading.

In this regard the dramatic difference in the $N1s(NO_2)$ core-hole spectrum of PNA on going from the vapor phase to the solid has recently been attributed to strong core-hole induced intermolecular orbital mixing.[14,15] Semiempirical equivalent-core computations were performed on model dimer structures chosen to reflect the experimental condensed phase intermolecular pairing, and provide the electronic reservoir for intermolecular screening. It was argued that orbital mixing effects resulted in an ionized dimer HOMO/LUMO separation significantly less than achieved in the isolated molecule case, indicating very low energy singly *and* doubly excited configurations. Estimates of the coupling parameters between the primary core-hole and the singly and doubly excited configurations of interest suggested a final-state energy and intensity distribution in relatively good agreement with experiment. Computations on the corresponding monomer core-hole suggested minimal contributions from doubly excited configurations due to their larger excitation energy. Analysis of the relative one-electron
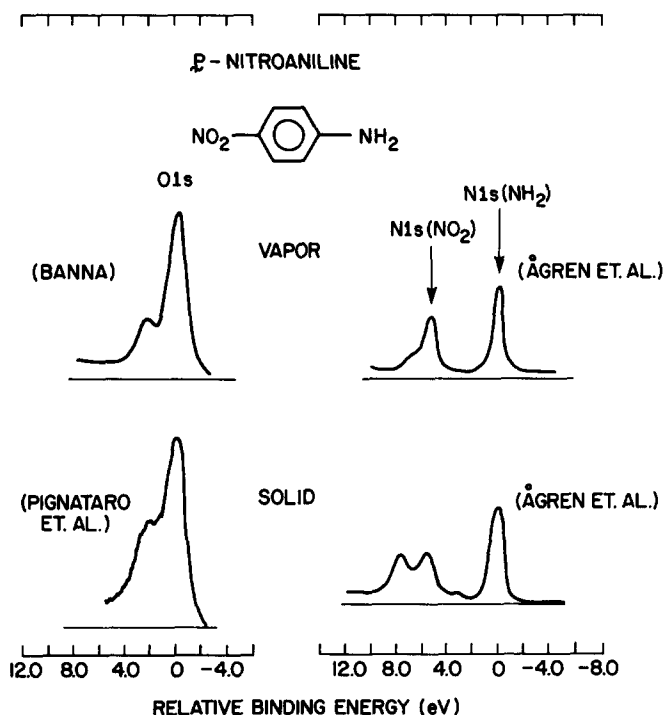


FIG. 1. The $N1s(NH_2)$, $N1s(NO_2)$, and $O1s(NO_2)$ vapor and condensed phase spectra of PNA, (a) $O1s$ vapor phase spectrum—Banna (Ref. 12), (b) $O1s$ condensed phase spectrum—Pignataro *et al.* (Ref. 3), (c) $N1s$ spectra—Ågren and co-workers (Ref. 25).

energies of the ionized species as compared to the surrounding neutral molecules considering the spatial separations in the crystal led to the rationalization that the PNA $O1s(NO_2)$ spectrum should be relatively unperturbed on going from the vapor to the condensed phase as observed experimentally.

Ågren and co-workers[25] have performed detailed *ab initio* computations on the $N1s(NO_2)$ ionization spectrum of PNA using a multiconfigurational self-consistent field (MCSCF) method and attribute the gas phase satellite structure essentially to the $\pi^* \leftarrow \pi$ HOMO $\rightarrow$ LUMO doubly excited configuration (CI coefficient 0.74). Ågren *et al.* emphasized that the $\pi^* \leftarrow \pi$ HOMO $\rightarrow$ LUMO singly excited *"singlet"-coupled* doublet provides only a minor contribution to the final primary hole state *and* low-lying satellite features of interest! As noted by Ågren and co-workers[25] these findings pose the fundamental question of whether even the vapor phase core-hole spectra of $D^+-Ar-A^-$ systems can be accurately reflected within a computational scheme limited to singly excited configurations. Although Ågren *et al.*[25] obtained excitation energies in good agreement with experiment, the intensity calculated for the satellite of interest is somewhat larger than found experimentally. Based on their isolated molecule results Ågren and co-workers[25] further suggested that the vapor to condensed phase $N1s(NO_2)$ spectral shifts may arise from hydrogen bonding interactions rather than strong core-hole induced intermolecular orbital mixing. It was argued that due to the relative sensitivity of the doubly excited configurations on the orbital separation the details of the final-state configuration interaction may be dramatically altered by relatively weak perturbations.

Ford and Hillier[21,30] also performed *ab initio* CI computations on $N1s(NO_2)$ *and* $O1s(NO_2)$ ionized PNA using a frozen orbital scheme $(FO-CI)^{21,30}$ and an explicit RHF hole-state basis set $(\Delta \text{ SCF-CI})$.[30] Both methods included selected doubly excited determinants in the CI expansions. Although both techniques produced a final-state spectrum (energy and intensity approximating experiment), the $\Delta$ SCF-CI method gave excitation energies and shake-up intensities in closer agreement with experiment. Contrary to the results of Ågren *et al.*,[25] Ford and Hillier found that the dominant contribution to the PNA $N1s(NO_2)$ and $O1s(NO_2)$ satellites of interest was the singly excited HOMO $\rightarrow$ LUMO configuration.

The purpose of this study is to further address the origin of the observed changes in the core-hole spectral functions on going from the gas to the solid phase for PNA in particular, and $D^+-Ar-A^-$ systems in general. To this end we report the vapor phase heteroatomic core-hole spectra of 2-amino-6-nitronaphthalene (2,6-ANN) and 1-amino-4-nitronaphthalene (1,4-ANN) and compare the results with the condensed phase spectra of Distefano and co-workers.[5] These systems were selected because the solid state core-hole spectrum of 2,6-ANN is one of the most unusual and complex observed thus far in that not only does the $N1s(NO_2)$ emission consist of two well-resolved peaks (Fig. 2), but the higher binding energy feature of the $N1s(NO_2)$ doublet structure is more intense than the "secondary" feature on the *lower binding energy side*. Recently other systems
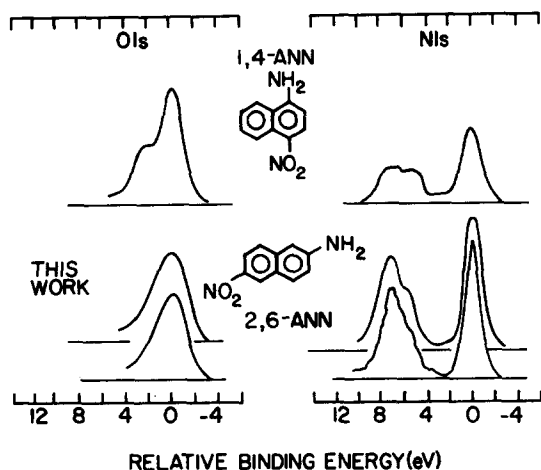
FIG. 2. The $N1s(NH_2)$, $N1s(NO_2)$, and $O1s(NO_2)$ condensed phase spectra of 1,4-ANN and 2,6-ANN taken from the work of Distefano *et al.* (Ref. 5). The solid state spectra taken during this work are shown for comparison.
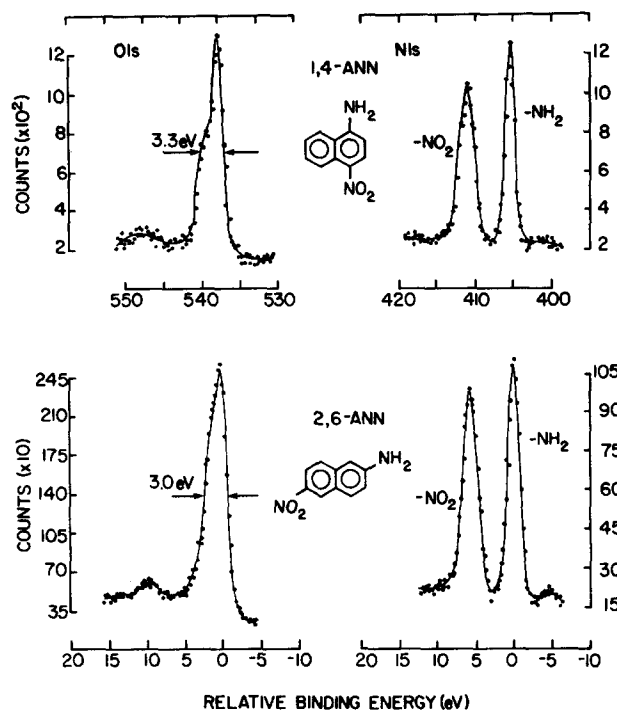


RELATIVE BINDING ENERGY (eV)

FIG. 3. The vapor phase core-level spectra of 1,4-ANN and 2,6-ANN. The absolute binding energy scale for 1,4-ANN, established as noted in the text, is included as an insert. The lines through the data points are included to serve as a guide, and do not correspond to formal curve resolution.

have been shown to yield similar solid state spectra.[23] 1,4-ANN, on the other hand, is found to exhibit an $N1s(NO_2)$ core-hole structure in the solid state parallelling PNA. As in the case of PNA, the vapor phase $N1s(NO_2)$ spectra are found to be considerably different from the solid state results.

CNDO/S(CI) equivalent-core computations including up to doubly excited configurations, were performed to establish the character of the monomer spectra, and to address the nature of the core-hole induced intermolecular interactions. X-ray crystallographic measurements on 2,6-ANN indicate an intermolecular donor/acceptor pairing scheme as in PNA. Dimer models are therefore constructed to computationally address the solid state interactions in PNA and 2,6-ANN.[14,15] The equivalent-core computations, with doubly excited configurations, yield final-state energy *and* intensity distributions for the $N1s(NO_2)$, $O1s(NO_2)$ and $N1s(NH_2)$ ionizations of PNA and 2,6-ANN, for both the monomer (vapor) and dimer (solid) species, in agreement with experiment. As in our previous studies we attribute the vapor to condensed phase spectral differences to strong core-hole induced intermolecular screening processes.[14–16] Similar intermolecular screening contributions have also been noted in the interpretation of the condensed phase spectra of $I_2$[34] and $NO$.[35,36]

## EXPERIMENTAL

Vapor phase XPS measurements on 2,6-ANN and 1,4-ANN were taken with $AlK_\alpha$ x-rays (1486.582 eV[37]) using a spectrometer at Vanderbilt University. Both compounds required heating to $\sim 140$ °C. The results for the $N1s$ and $O1s$ core regions are shown in Fig. 3. Binding energies for 1,4-ANN were determined using the neon $KL_{2,3}L_{2,3}$ ($^1D_2$) line [804.50(3) eV[38]] for $O1s$ and the $N1s$ line of $N_2$ for $N1s$ (409.93 eV[37]). The latter calibration was somewhat uncertain due to the overlap between the $N1s$ level of $N_2$ and that of the amino group. The relative intensities and energies for both compounds obtained by least-squares fitting Lorentzian or

Gaussian functions to the data points[39] are given in Table I. The $O1s$ binding energy of the most intense peak in 1,4-ANN is identical to that measured for PNA.[27] This probably means that there is a somewhat greater relaxation energy associated with $O1s$ ionization in 1,4-ANN than the corresponding ionization in PNA, since the average energy of the core ionization spectrum is known to correspond to the ionization energy obtained in accord with Koopmans' theorem.[31(b)] Thus the difference between the mean energy and the energy of the main peak reflects the relaxation energy. The mean energy for the $O1s$ region in 1,4-ANN is *prob-*

TABLE I. Experimental binding energies and relative intensities for vapor phase core-level ionization of 2,6-ANN and 1,4-ANN.

| | Level | Binding energy(eV) | Relative intensity |
|---|---|---|---|
| 2,6-ANN | $N1s(NH_2)$ | 0 | 1.0 |
| | $N1s(NO_2)$ Satellite(s) | 5.8(1) | 1.0 |
| | $O1s$ | 0 | 1.0 |
| | Satellite 1 | 1.4(2)[a] | 0.6(1)[a] |
| | Satellite 2 | 10.0(2) | ~0.1 |
| 1,4-ANN | $N1s(NH_2)$[b] | 0 | 1.0 |
| | $N1s(NO_2)$ Satellites | 5.8(1) | 0.9 |
| | $O1s$[c] | 0 | 1.0 |
| | Satellite 1 | 1.9(2)[a] | 0.5(1)[a] |
| | Satellite 2 | 9.7(2) | ~0.1 |

[a] Values obtained by fitting two peaks of equal FWHM to the main peak.

[b] An absolute binding energy of 405.5(2) eV has been obtained using $N_2$ as calibrant (see Fig. 3).

[c] An absolute binding energy of 537.9(2) eV has been obtained using neon $KL_{2,3}L_{2,3}$ ($^1D_2$) as calibrant (see Fig. 3).

*ably* greater than that in PNA since the main satellite peak appears about twice as intense as in PNA, while the separations from the main peak are comparable (~2.0 eV in 1,4-ANN and ~2.4 eV in PNA.) It is quite reasonable to expect greater relaxation in 1,4-ANN due to the more extensive ring system compared to PNA. On the other hand, the N1$s$ binding energies are ~0.5 eV lower in 1,4-ANN than in PNA; which means that the amino–nitrogen binding energy in 1,4-ANN is very close to that in aniline.[40] We also found the peak due to the N1$s$(NO$_2$) ionization to be ~0.4 eV broader than the corresponding–NH$_2$ derived peak in 2,6-ANN, compared to an ~0.7 eV difference in 1,4-ANN.

Comparison solid state XPS measurements were performed on 2,6-ANN using an AEI ES200B photoelectron spectrometer (normal operating pressure ~10$^{-8}$ Torr). Photoelectron spectra were accumulated using an unfiltered Mg$K_\alpha$ source ($\hbar\omega$ = 1253.7 eV). 2,6-ANN were applied in powder form directly to the probe tip and wetted with acetone to promote adhesion. Residual acetone was purged from the sample by rough pumping prior to insertion into the spectrometer high vacuum (the typical pressure during data accumulation was 1.1×10$^{-8}$ Torr). The comparison spectra shown in Fig. 2 parallels the published work of Distefano and co-workers.

Crystals of 2,6-ANN (density = 1.442 g cm$^{-3}$) were found to be monoclinic with cell constants $a$ = 10.4877(7) Å, $b$ = 6.1216(6) Å, $c$ = 14.164(2) Å, $\beta$ = 107.58(1)°, $Z$ = 4 and space group $P_2n$. By means of a computer controlled EN-RAF-NONIUS CAD 4 diffractometer all reflections with $\theta$ < 30° (Mo$K_\alpha$ graphite monochromator) were measured at room temperature. 1207 independent reflections with $I$>2$\sigma$(I) were considered to establish the molecular structure of 2,6-ANN shown in Fig. 4. The intensities and their standard deviations were corrected for Lorentz and polarization effects, but were used without absorption correction. The structure was solved by direct methods and refined by a least squares fit using the program package SHELX.[41] The refinement index decreased to $R$ = 0.041 for 1207 reflections. H-atom positions were derived from difference maps and refined isotropically together with C and N atoms. The final thermal parameters and fractional atomic coordinates, and a list of observed and calculated structure factors are available upon request (JL). A complete tabulation of the bond lengths

and bond angles according to the structure of Fig. 4 is given in the Appendix.

To illustrate the molecular packing Fig. 5(a) shows the projection along the $b$ axis onto the $a$–$c$ plane. The structure is widely analogous to the one reported by Trueblood and Donahue for $p$-nitroaniline.[42] Figure 5(b) illustrates the closest contact between a chosen NH$_2$ group on one end of the molecule and surrounding groups on other moieties. Each NH$_2$ group has two nearest neighboring NO$_2$ groups as in PNA. The separation of 3.13/3.14 Å in 2,6-ANN compares favorably with the value of 3.08 Å found in PNA.[42]

2,6-ANN and 1,4-ANN were obtained from ICN Pharmac. Inc., Plainview, New York and used without additional purification. As a precaution against anomalous effects due to sample preparation we separately synthesized 2,6-ANN. Both 2,6-ANN sources yielded consistent vapor and condensed phase XPS spectra. The x-ray crystallographic measurements were taken on our synthesized material.

## COMPUTATIONAL

Calculations were performed within the semiempirical all-valence-electron closed-shell CNDO/S formalism[43–45]
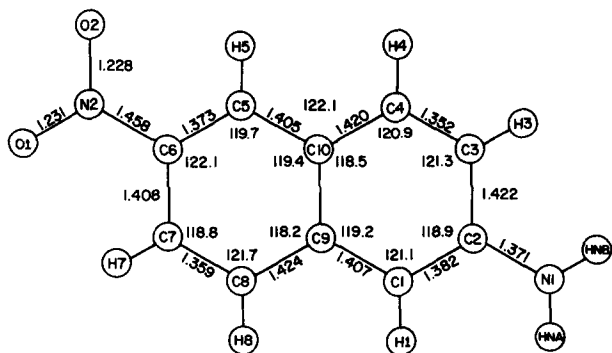


(a)

(b)



FIG. 4. Partial bond angles and bond lengths obtained from the crystal structure determination of 2,6-ANN. The atomic numbering system is also indicated.
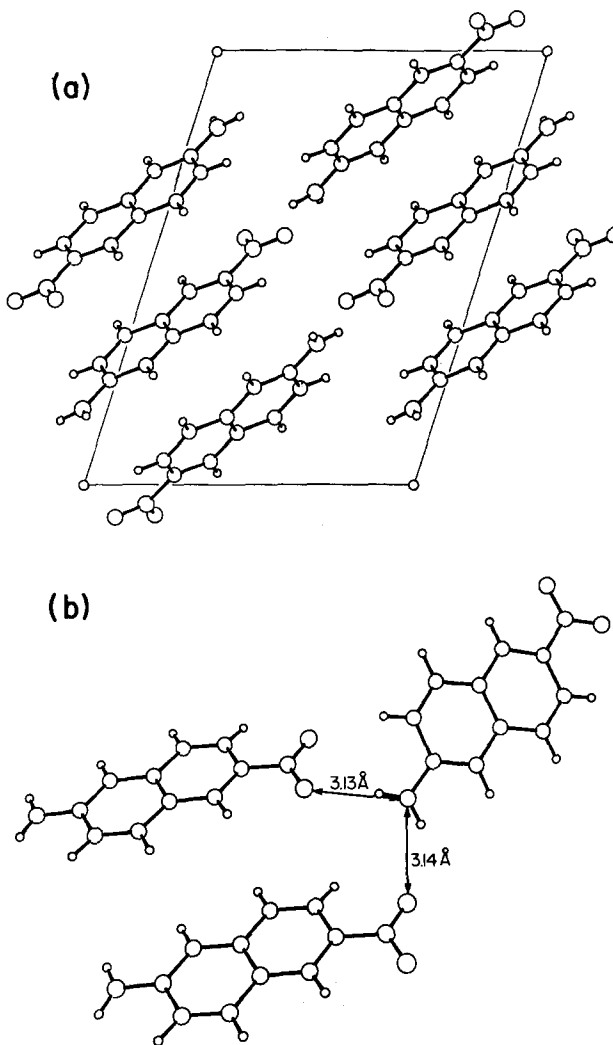
FIG. 5. (a) The projection of 2,6-ANN along the $b$ axis onto the $a$–$c$ plane, (b) the closest contact between the NH$_2$ group and surrounding groups on nearest moieties.

including up to doubly excited configurations[46] using the Pariser–Parr approximation to the two-center Coulomb repulsion integrals.[47] Core-ionized species were treated within the equivalent-core approximation[48,49] where the atom to be ionized (atomic number $Z$) was replaced by the next highest atom in the periodic table $(Z' = Z + 1)$. Convergence was achieved for all $N1s(NO_2)$, $O1s(NO_2)$, and $N1s(NH_2)$ monomer and dimer configurations considered. Excited state computations were then performed on the "equivalent-core" closed-shell species assuming only singlet coupling between all valence electrons. Due to the complexity introduced by including doubly excited configurations no attempt was made to approximate exchange interactions between the core and valence electrons. It has been demonstrated for $D^+$–$Ar$–$A^-$ systems that the triplet-coupled doublet manifold generally yields "small" contributions to the calculated spectra when large intensity secondary features are present.[14,21,24,25,28–30] It is assumed that neglect of triplet coupling in the present study does not lead to serious deficiencies in spectral interpretation. Although our approach involves a number of approximations, the results appear to adequately simulate response of the valence electrons toward the core holes in both the monomer and dimer configurations.

In all ionic-state calculations which include doubly excited state configurations (explicitly noted in the text) the 300 lowest energy excitations were selected from 5000 created configurations of proper symmetry. Relative intensities were obtained by projection of the correlated ion-state wave function onto the "uncorrelated" (see below) wave function of the neutral system according to the sudden approximation[31,50,51]

$$I_i^{rel} \alpha |\langle \Psi_{i,final}^{ion} | \Psi_{initial}^{ion} \rangle|^2. \tag{1}$$

Within this approximation a sum rule holds which equates the first moment of the spectral function to the Hartree–Fock eigenenergy[31(b)]

$$E_{HF} = \sum_i (E_i^{ion} - E^{ion}) I_i^{rel}. \tag{2}$$

This relationship permits us to calculate relaxation energies since this quantity is given as the difference between the Hartree–Fock eigenenergy and the true ionization potential.

It has been found that accurate intensity calculations on small molecules require a correlated neutral molecule wave function.[52–55] Our CNDO/S(CI) results, however, indicate a relatively pure single determinant solution for the PNA neutral molecule ground state—a 95.7% SCF configuration using Pariser–Parr two-center integrals; a 91.6% SCF configuration using Nishimoto–Mataga integrals.[56] Since Pariser–Parr integrals are used in the generation of the ion states and the reference neutral molecule wave function for intensity evaluation we feel justified in neglecting correlation contributions to the neutral species considered in this study. It should be noted, however, that the *ab initio* study of Ågren *et al.*[25] does find rather large PNA neutral molecule ground state correlation (84.6% SCF configuration).

Intramolecular atomic coordinates used in the computations were calculated from the bondlengths and bond angles given by Pople and Beveridge.[57] Intermolecular separa-

tions were chosen to reflect experiment (see appropriate figures). Comparison neutral molecule and equivalent-core calculations were performed on PNA, 1,4-ANN, and 2,6-ANN using singly excited configurations and the Nishimoto–Mataga repulsion integrals. Variations in parameter options are clearly indicated in the text.

## RESULTS AND DISCUSSION

### *p*-nitroaniline (PNA)

Our computational results on the monomer and dimer heteroatomic core-level ionizations of PNA are given in Fig. 6. As observed experimentally (Fig. 1) the $N1s(NO_2)$ monomer ionization yields only a relatively weak asymmetric structure on the high binding energy side of the primary peak $(\Delta E = 1.73 \text{ eV}; \Delta E_{EXP} = 1.25 \text{ eV})$. In the dimer configuration the $N1s(NO_2)$ core-hole spectrum exhibits a well-resolved double peak structure of approximately equal intensity $(\Delta E = 2.35 \text{ eV}; \Delta E_{EXP} \simeq 2.0 \text{ eV})$. The $O1s(NO_2)$ final-state distributions indicate a relatively strong shake-up feature at $\sim 2.8$ eV which is moderately enhanced in intensity on going to the dimer model. The $N1s(NH_2)$ spectrum in both the monomer and dimer configurations is composed of a single intense peak. Our model calculations, therefore, reflect the fundamental vapor phase to solid state core-hole energy and intensity distributions observed experimentally.

Table II shows that for the $N1s(NO_2)$ monomer ionization the doubly excited $\pi^* \leftarrow \pi$ HOMO $\rightarrow$LUMO equivalent-core configuration remains approximately 3.0 eV above the corresponding singly excited excitation. Localizations of the equivalent-core orbitals which contribute most strongly to the shake-up interpretation are given in Fig. 7. In terms of these few orbitals shake-up excitation can be viewed essen-
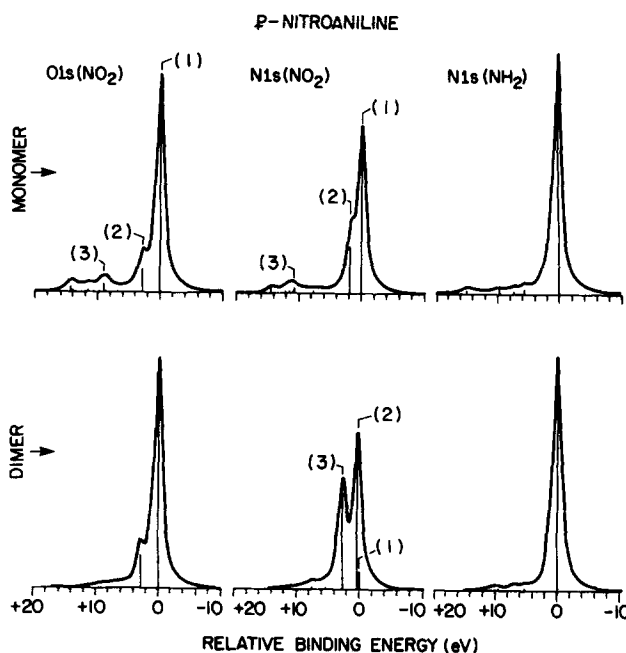


FIG. 6. The theoretical monomer and dimer $N1s(NO_2)$, $O1s(NO_2)$, and $N1s(NH_2)$ core-hole spectra of PNA obtained using correlated ion states.

TABLE II. Computational results on the PNA N1$s$(NO$_2$) monomer core hole. Determinant character is represented by ($a,b$ $\|$ $c,d$) where $a \rightarrow d$ and $b \rightarrow c$ excitation has occurred relative to the closed-shell ion state (0,0 $\|$0,0).

| Contributing determinants | | | |
|---|---|---|---|
| Order | Determinant(DET) | $\langle \Psi^{a \rightarrow d}_{b \rightarrow c}(I)| \Psi_{GS}(N)\rangle$ | $E_{DET}$(eV) |
| 1 | (0,0 $\|$0,0) | 0.736 58 | 0.0 |
| 2 | (0,26 $\|$ 27,0) | − 0.272 19 | 3.22 |
| 3 | (0,26 $\|$ 28,0) | − 0.073 20 | 5.52 |
| 4 | (26,26 $\|$ 27,27) | 0.100 58 | 6.13 |
| Final-state distribution | | | |
| State | (0,0 $\|$ 0,0) CI coefficient | $|\langle \Psi_F(I)|\Psi_{GS}(N)\rangle|^2$(%) | $E^F$(eV) |
| 1 | − 0.937 67 | 42.95 | 0.0 |
| 2 | − 0.143 31 | 12.77 | 1.73 |
| 3 | − 0.095 48 | 1.40 | 10.71 |
| State | Wave function (CI vector) | | |
| 1 | − 0.93767(0,0 $\|$0,0) + 0.23401(26,26 $\|$ 27,27) + ··· | | |
| 2 | − 0.14331(0,0 $\|$0,0) + 0.77529 (0,26 $\|$ 27,0) − 0.14267(0,26 $\|$ 28,0) − 0.47150(26,26 $\|$27,27) + ··· | | |

tially as a transition leading to charge-transfer from the − NH$_2$ donor fragment to the −NO$_2$ acceptor moiety as indicated in previous studies. Within the present basis set, however, the singly excited ion-state HOMO →LUMO excitation "separately" accounts for only a small portion of the shake-up intensity. For example, assuming a pure one-elec-
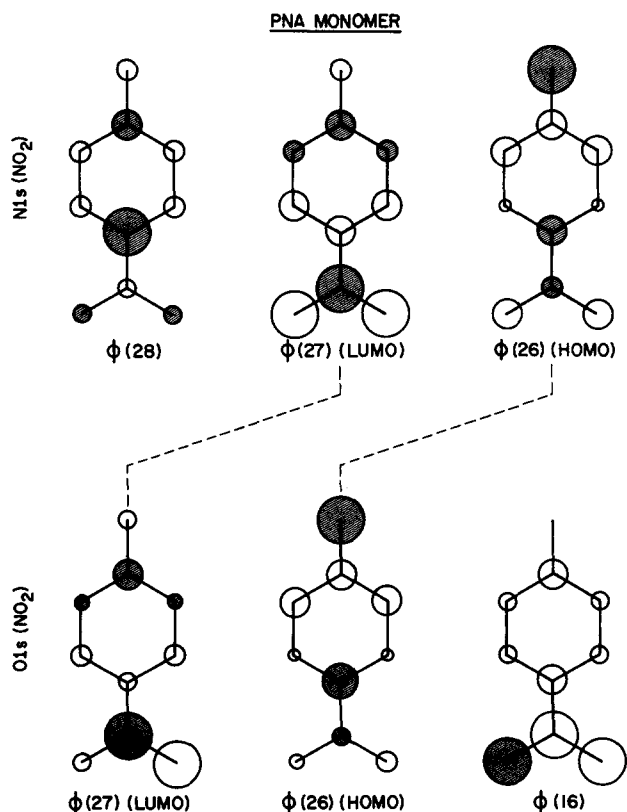
**PNA MONOMER**



FIG. 7. The PNA monomer ion-state orbitals relevant to the discussion of the N1$s$(NO$_2$) and O1$s$(NO$_2$) core-hole spectra. The orbital lobes are drawn proportional to the LCAO coefficients and viewed from above the molecular plane.

tron HOMO →LUMO interpretation of the N1$s$(NO$_2$) shake-up a relative intensity of only 13.7% is obtained from the determinantal overlaps given in Table II compared to the final-state value of 29.7%. The shake-up transition gains the appropriate additional intensity through constructive interference effects between the singly excited HOMO →LUMO, and the ionic ground state and doubly excited configurations contributed through final-state CI. Final-state CI also refines the energy spectrum to that observed experimentally. It should be noted that the value of the squared overlap integral $|\langle (0,0 \| 0,0)_I |(0,0 \| 0,0)_N \rangle|^2$ for N1$s$(NO$_2$) ionization is 0.54. The $\Delta$ SCF-CI results of Ford and Hillier[30] yield 0.53 for the corresponding projection, from which a relative shake-up intensity of 23% is obtained. Our analysis also yields a small overlap between the neutral molecule ground state and the ion-state determinant formed by double excitation from the HOMO to the LUMO level.

In addition to assigning a large HOMO →LUMO doubly excited character to the N1$s$(NO$_2$) shake-up transition as noted in the Introduction, Ågren *et al.*[25] argue for significant final-state CI contributions from doubly excited configurations between the 1$a_2(\pi)$ occupied orbital localized on the oxygen atoms and the 5$b_1(\pi^*)$ LUMO orbital; levels which they term "near degenerate." Such "near degeneracy" is also apparent in their neutral molecule ground state calculation where the CI coefficient for the 5$b^2_1(\pi^*) \leftarrow 1a^2_2(\pi)$ double substitution is approximately a factor of 3 larger than the next highest excited state contribution. Ågren *et al.*[25] emphasized the importance of such doubly excited contributions in understanding the details of intramolecular core-hole screening. Our CNDO/S calculations yield 5$b_1(\pi^*) \leftarrow 1a_2(\pi)$ and 5$b^2_1(\pi^*) \leftarrow 1a^2_2(\pi)$ transition energies of ~6.0 and > 12.0 eV, respectively, in the neutral molecule. In accord with symmetry considerations only the doubly excited component can couple with the ground or the ion-states of interest. As shown above, however, coupling with the neutral ground state is negligible. Due to the relative localizations our ion-state computation shows an ~2.5 eV *decrease* in the difference between the 5$b_1(\pi^*)$ and 1$a_2(\pi)$ orbital eigenvalues when compared to those of the neutral species, yielding a 5$b^2_1(\pi^*) \leftarrow 1a^2_2(\pi)$ transition energy of ~7.0 eV. The wave function for the intense shake-up transition given in Table II contains only the major components derived from transitions with energies $\leq$6.25 eV. Although most of the shake-up intensity is accounted for in terms of the indicated components, the contributions given in Table II reflect only ~86% of the total wave function. We arbitrarily chose to tabulate CI vectors only for the 30 lowest-energy configurations derived from an excitation manifold containing all possible symmetries. As demonstrated below, however, our ion-state computations also reflect significant coupling to excitations out of the 1$a_2(\pi)$ orbital.

In order to illustrate the nature of the ion-states which lead to the observed N1$s$(NO$_2$) spectral function appropriate electron density difference plots are given in Fig. 8. Figure 8(a) shows the differences between the ionic core-hole ground state and the ground state of the neutral system. Solid lines represent electron gain in the ion, whereas dashed lines correspond to electron loss. The surface on which the
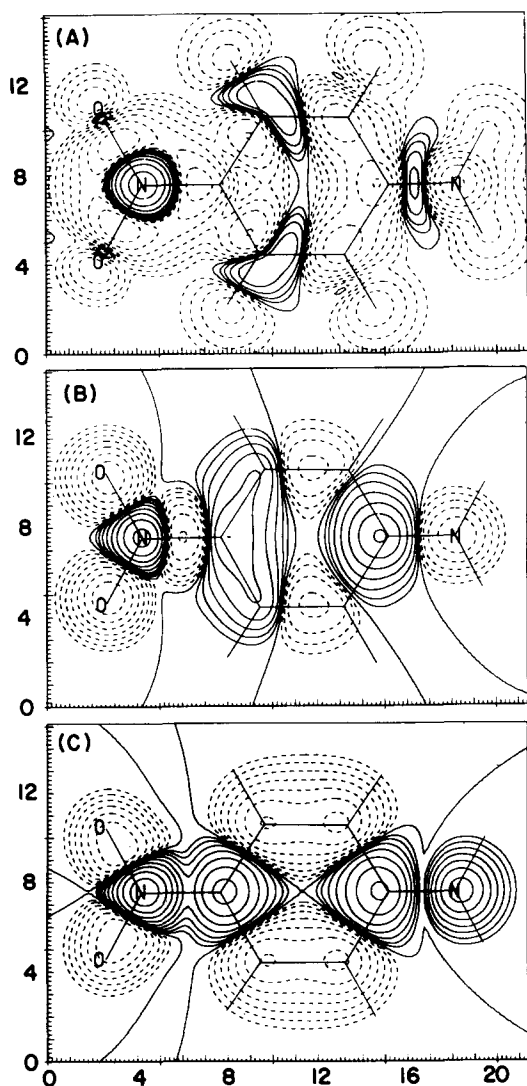
FIG. 8. Electron density difference plots for the ionic ground and excited states of PNA with a N1s hole on the $NO_2$ group: (a) $\rho(PNA^+$, ground state) $- \rho(PNA$, neutral); (b) $\rho(PNA^+$ state #2) $- \rho(PNA^+$, ground state); (c) $\rho(PNA^+$, state #3) $- \rho(PNA^+$, ground state).

electron densities are indicated lies 0.5 Å above the molecule in order to include changes in $\pi$-electron density for which the molecular plane corresponds to a nodal plane. Clearly the plot shows a screened ionic ground state, where a screening charge of $\sim 0.93e$ accumulates on the ionized nitrogen atom. Note that the screening charge is drawn from all parts of the molecule. Upon electron excitation into the most intense shake-up state the electronic charge further rearranges. This is indicated in Fig. 8(b) where the difference has been taken between the excited and ground states of the ion. The excited state in Fig. 8(b) exhibits an approximately $0.13e$ greater intramolecular screening at the ionized nitrogen atom than calculated for the ionic ground state. Excited state screening occurs primarily through electron transfer from the $-NH_2$ donor group, *and from the adjacent oxygen atoms* in line with the interpretation of Ågren and co-workers.[25] Figure 8(b) obviously reflects significant $5b\,{}^2_1(\pi^*)\!\leftarrow\!1a^2_2(\pi)$ contribution to the shake-up state which was overlooked in our truncation of the wave function output. The component

of intramolecular screening arising from charge transfer from the oxygen atoms is entirely a many-body effect. In contrast, significant charge transfer *to the oxygen centers* is expected based on a one-electron interpretation as indicated from the relative HOMO/LUMO localizations given in Fig. 7. An additional example of electron rearrangement is given for a higher-lying shake-up state in Fig. 8(c). In this case all atoms on the molecular axis exhibit greater screening relative to those lying off axis.

Table III indicates that the $O1s(NO_2)$ monomer spectrum can be viewed as a relatively pure hole state with $\sim 65\%$ of the shake-up transition due to the one-electron intramolecular charge-transfer HOMO $\rightarrow$ LUMO excitation (Fig.7). Our final-state calculation, however, yields only a 10.70% relative intensity for the $O1s(NO_2)$ shake-up, compared to the experimental value of 24%. Furthermore, although the HOMO $\rightarrow$ LUMO configuration participates strongly in the description of the shake-up state, such one-electron excitation contributes only 3.8% relative intensity due to the relatively small $(0,26||27,0)$ overlap with the neutral molecule ground state. We attribute the small calculated shake-up intensity to: (i) O1s hole localization, and (ii) neglect of the small correlation contribution to the neutral molecule ground state noted above. Symmetry adapting the O1s hole state to preserve the $C_{2v}$ symmetry of the molecule, as well as inclusion of neutral molecule correlation contributions may lead to a greater projection amplitude, thus enhancing the calculated satellite intensity. As in the case of $N1s(NO_2)$ ionization a considerable portion of our calculated $O1s(NO_2)$ shake-up intensity arises from positive CI coupling (when the determinantal overlap factors are included) between the excited and ionic ground state configurations. In comparison, Ford and Hillier[30] likewise evaluated the O1s hole-state spectrum assuming reduced symmetry. The present squared ground state projection (0.635) compares

TABLE III. Computational results on the PNA $O1s(NO_2)$ monomer core hole.

| | Contributing determinants | | |
|---|---|---|---|
| Order | Determinant(DET) | $\langle \Psi^{a\rightarrow d}_{b\rightarrow c}(I)|\Psi_{GS}(N)\rangle$ | $E^{DET}$(eV) |
| 1 | $(0,0\ \|\ 0,0)$ | 0.796 89 | 0.0 |
| 2 | $(0,26\ \|\ 27,0)$ | $-0.186\ 08$ | 3.83 |
| 3 | $(0,16\ \|\ 27,0)$ | 0.224 26 | 9.14 |

| | Final-state distribution | | |
|---|---|---|---|
| State | $(0,0\ \|\ 0,0)$ CI coefficient | $|\langle\Psi_F(I)|\Psi_{GS}(N)\rangle|^2$(%) | $E^F$(eV) |
| 1 | 0.974 96 | 57.84 | 0.0 |
| 2 | 0.104 56 | 6.16 | 2.68 |
| 3 | 0.019 63 | 2.40 | 8.92 |

| State | Wave function (CI vector) |
|---|---|
| 1 | $0.974\ 95\ (0,0\ \|\ 0,0) + \cdots$ |
| 2 | $0.104\ 56\ (0,0\ \|\ 0,0) - 0.80582\ (0,26\ \|\ 27,0) + \cdots$ |
| 3 | $0.019\ 63\ (0,0\ \|\ 0,0) + 0.64309\ (0,16\ \|\ 27,0) + \cdots$ |

favorably to their FO-CI value of 0.64 which produced a relative shake-up intensity also considerably less than experiment (13%). Although the $\Delta$ SCF-CI results of Ford and Hillier[30] accurately reflects the $N1s(NO_2)$ spectrum, the relative $O1s$ shake-up intensity is calculated to be too large by approximately the same amount as the underestimation in their FO-CI model ($\sim 10\%$).

It is interesting to address the results of two prior CNDO/S equivalent-core studies on PNA which were restricted to singly excited configurations, and which reported $N1s(NO_2)$ and $O1s(NO_2)$ shake-up strengths approximating experiment. Our earlier work essentially used the *absolute* intensity approximation of Darko, Hillier, and Kendrick[58] where $O1s(NO_2)$ and $N1s(NO_2)$ shake-up intensities of 20%→25% and ~38%→40%, respectively, where obtained assuming only singly excited configurations and an independent term-by-term evaluation of neutral/ion-state orbital overlaps between appropriate levels given in the configuration interaction expansion.[14] These results compare favorably with the intensities calculated earlier by Distefano and co-workers where intensity evaluation using complete determinant projection was implied.[13] Based on our present computations, which yield appropriate determinantal overlaps involving singly excited configurations considerably less than suggested by two-level techniques, it appears that Distefano *et al.*[13] likewise truncated determinant projection to evaluate intensities. Distefano and co-workers have, in fact, calculated the shake-up structure for a wide variety of donor/acceptor molecules within the CNDO/S equivalent-core approach using only singly excited configurations with apparent two-level intensity projection, and generally found excellent correspondence with experiment.[13,17,19,20] Our recent work[16,24,59] on the shake-up structure of additional organic systems parallel the conclusions drawn by Distefano *et al.* It should be noted that Distefano *et al.*[13] originally emphasized that the theoretical intensities for acceptor $O1s$ shake-up were generally a factor of 2 lower than observed for a variety of $D^+$-Ar-$A^-$ systems, whereas acceptor $N1s$ intensities were reproduced quite accurately. As indicated above, these conclusions also extend to our findings using the more complete doubly excited basis set with full determinant projection. Based on the present results, however, it can be concluded that while singly excited approaches with truncated intensity projections are often useful in identifying the "primary" configurations responsible for shake-up features in simple $D^+$-Ar-$A^-$ systems, the details of the final-state interactions may be incomplete and even misleading. For example, the PNA $O1s(NO_2)$ spectrum calculated by Distefano *et al.*[13] yields a higher-energy shake-up feature more intense than that due to HOMO →LUMO excitation. The results given in Table III indeed parallel the spectrum of Distefano *et al.*[13] provided final-state configuration interaction is ignored. When interactions with the ion ground state are included the shake-up feature characterized by HOMO →LUMO excitation appears with approximately three times greater intensity than the higher-energy component.

Figure 9 and Table IV indicates that each of the three final-states contributing to the $N1s(NO_2)$ dimer spectrum are composed in large part of configurations derived from
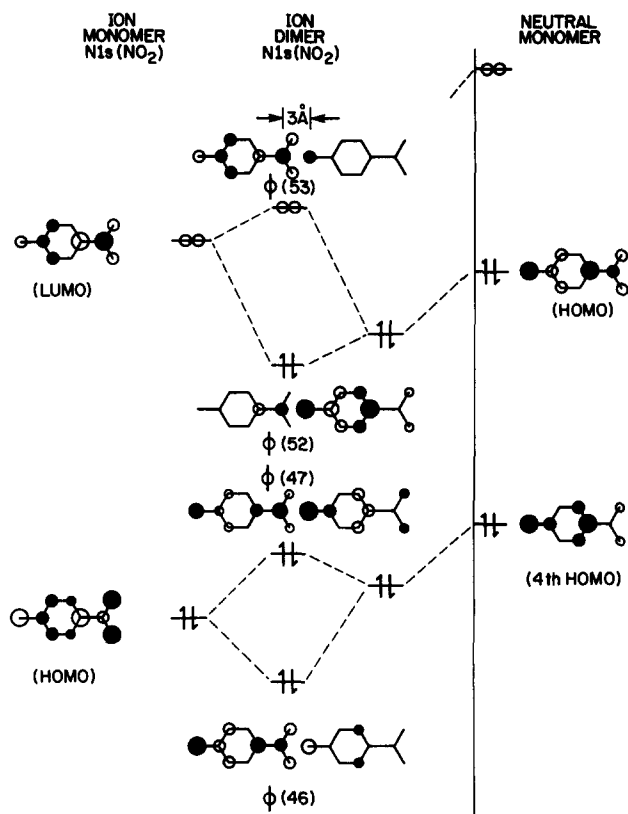


FIG. 9. The PNA $N1s(NO_2)$ dimer orbitals of interest in terms of the neutral and ionic monomer components.

intermolecular charge transfer from the "neutral" component. The two lowest energy states are essentially destructive and constructive combinations, respectively, of the ground and singly excited HOMO →LUMO configurations. The lowest energy state, however, has the dominant HOMO →LUMO character (48.1%). Although the three lowest energy final states do not contain a dominant doubly excited configuration, the importance of the double substitutions is dramatically illustrated in the dimer model. It is important to note in this regard that the initial configurations which contribute most heavily to the $N1s(NO_2)$ shake-up interpretation, (0,26 || 27,0) in the monomer and (0,46 || 53,0) in the dimer, are approximately energetically degenerate! Using one-electron energies, for example, and appropriate determinantal overlaps yields an $N1s(NO_2)$ dimer spectrum with relative intensities of 0.0 eV (47.6%), 0.95 (2.2%), and 3.02 eV (7.3%). The four dominant configurations comprising the final-state #3 wave function exhibit positive interference in the intensity computation when the signs of the determinantal overlap factors are included. Although the indicated configurations individually contribute intensity in the range of 0.1% → 4.1%, when summed in the proper manner a shake-up feature with 22.66%, or 65.5% of the "main peak" intensity, is obtained. Although this value is somewhat less than experiment, our dimer results clearly reflect the double peak solid state structure with apparent increased splitting relative to the vapor phase. The calculated splitting of the $N1s(NO_2)$ dimer spectrum also appears overestimated

TABLE IV. Computational results on the PNA $N1s(NO_2)$ dimer core hole.

| | | Contributing Determinants | |
|---|---|---|---|
| Order | Determinant(DET) | $\langle \Psi_{b\rightarrow c}^{a\rightarrow d}(I) | \Psi_{GS}(N) \rangle$ | $E^{DET}(eV)$ |
| 1 | (0,0 ‖ 0,0) | 0.689 616 | 0.0 |
| 2 | (0,52 ‖ 53,0) | 0.149 219 | 0.95 |
| 3 | (0,47 ‖ 53,0) | − 0.074 820 | 2.67 |
| 4 | (0,46 ‖ 53,0) | − 0.270 241 | 3.02 |
| 5 | (46,52 ‖ 53,53) | − 0.058 475 | 5.18 |
| 6 | (46,46 ‖ 53,53) | 0.105 899 | 5.56 |

| | Final-state distribution | | |
|---|---|---|---|
| State | (0,0 ‖ 0,0) CI coefficient | $|\langle \Psi_F(I) | \Psi_{GS}(N) \rangle|^2 (\%)$ | $E^F(eV)$ |
| 1 | 0.5324 | 4.24 | 0.0 |
| 2 | − 0.7678 | 30.39 | 0.31 |
| 3 | − 0.2930 | 22.66 | 2.66 |

| State | Wave function (CI vector) |
|---|---|
| 1 | 0.532 38 (0,0 ‖ 0,0) − 0.69 376 (0,52 ‖ 53,0) − 0.206 41 (0,47 ‖ 53,0) <br> + 0.146 20 (0,46 ‖ 53,0) + 0.269 76 (46,52 ‖ 53,53) <br> − 0.106 60 (46,46 ‖ 53,53) + ⋯ |
| 2 | − 0.767 80 (0,0 ‖ 0,0) − 0.489 10 (0,52 ‖ 53,0) − 0.237 35 (0,47 ‖ 53,0) <br> + 0.214 35 (0,46 ‖ 53,0) + ⋯ |
| 3 | − 0.292 97 (0,0 ‖ 0,0) + 0.391 96 (0,47 ‖ 53,0) + 0.728 26 (0,46 ‖ 53,0) <br> − 0.345 78 (46,46 ‖ 53,53) + ⋯ |

by ~0.35 eV. We attribute this "enhancement" of the splitting to the intermolecular separation used in the computation (Fig. 9) which is somewhat reduced relative to the experimental spacing [Fig. 5(b)].

The dimer orbital correlation diagram for $N1s(NO_2)$ ionization is given in Fig. 9. As indicated, strong core-hole induced intermolecular orbital mixing occurs in the dimer. We previously rationalized the well-resolved solid-state doublet by suggesting a strong splitting between the ionic ground state and the one-electron HOMO →LUMO dimer excitation induced by coupling to low-lying doubly substituted configurations.[14,15] While indeed mixing between the HOMO level of the neutral part and the LUMO level of the ionic part gives a low energy excitation as indicated previously, the final-state which is defined in this work as the shake-up transition is mainly derived from excitations out of orbitals created by mixing between the HOMO level of the ion and the lower-lying occupied orbital also localized on the $-NH_2$ moiety of the neutral fragment. Although our previous $N1s(NO_2)$ dimer calculations (performed on a slightly displaced monomer pair) yielded a somewhat different magnitude of orbital mixing, it is shown in the following section that moderate geometry changes are not expected to dramatically alter the final-state spectrum.

Again the spectral function is analyzed in terms of electron density difference plots in an effort to relate the dimer transitions to those in the monomer. Figure 10(a) shows the electron rearrangement within the dimer upon coupling two noninteracting (neutral) PNA moieties self-consistently. Clearly the $\pi$-electron density of the monomer bearing the interacting $-NH_2$ group is the most strongly influenced. The effective charge flux between the molecules, however, is rela-

tively small (~0.05 $e$ per moiety). This is reflected in the magnitude of the dimer dipole moment which increases by only 3% relative to the sum of the dipole moments of the separated molecules. Since the details of charge rearrangement concomitant with ionization of the free molecule has been indicated in Fig. 8, we elect to refer charge rearrangements in the ionized dimer to a hypothetical charge density created by superimposing the densities of noninteracting neutral and $N1s(NO_2)$ ionized monomers. Figure 10(b) displays the difference between the electron densities of the $N1s(NO_2)$ ionized dimer ground state and the reference density distribution. As indicated, the ionic ground state exhibits strong intermolecular charge-transfer screening. Such a state therefore has little monomer equivalence and contributes only moderately to the spectral function as indicated in Fig. 6 and Table IV. The electron density of the intense dimer shake-up state #2 is plotted in Fig. 10(c) relative to the reference distribution. In addition to an obvious partial correspondence with the ionized monomer ground state, state #2 is characterized by an intermolecular screening contribution as well as a substantial intramolecular rearrangement of charge on the ionized portion. Figures 10(a) and 10(c) show a similar electron density difference pattern on the neutral dimer component indicating that state #2 can be characterized as the monomer ionic ground state moderately interacting with the neighboring neutral molecules. It appears that such interaction is sufficient to determine the spectral function. A similar situation is encountered in an analysis of the second intense dimer shake-up state (state #3). The neutral component in Fig. 10(d) exhibits nearly the same density difference structure as shown in Figs. 10(a) and 10(c), while the ionized portion yields a pattern similar to the
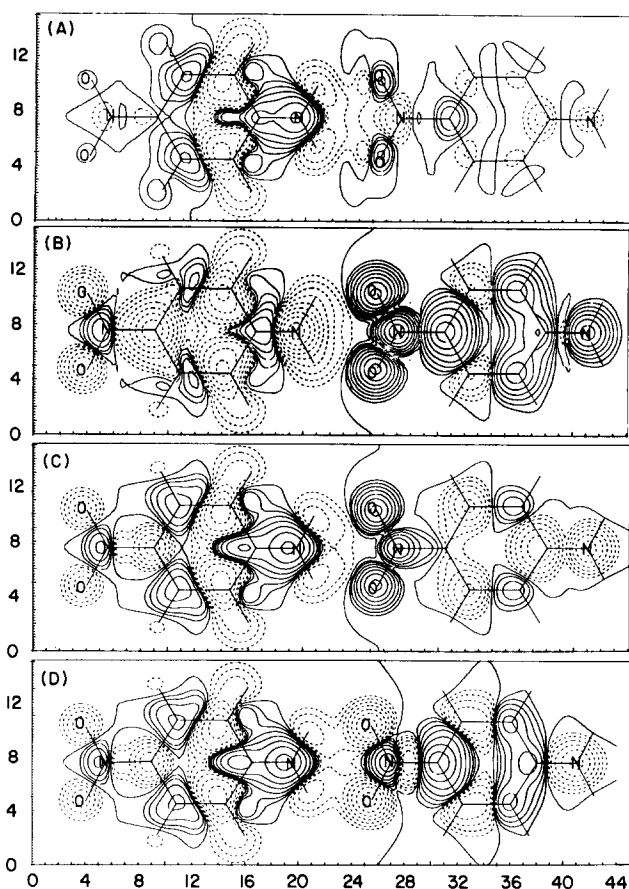
FIG. 10. Electron density difference plots between the neutral and ionic ground and excited states of the PNA dimer with an N1s hole on the interacting $NO_2$ group: (a) $\rho(PNA_2$, SCF coupled) $- \rho(PNA_2 -$ SCF uncoupled); (b) $\rho(PNA - PNA^+$, SCF coupled, ground state) $- \rho(PNA - PNA^+$, SCF uncoupled); (c) $\rho(PNA - PNA^+$, SCF coupled, state #2) $- \rho(PNA - PNA^+$, SCF uncoupled); (d) $\rho(PNA - PNA^+$, SCF coupled, state #3) $- \rho(PNA - PNA^+$, SCF uncoupled).

shake-up difference density in the monomer [Fig. 8(b)]. We therefore conclude that the two $N1s(NO_2)$ peaks observed in the gas phase correspond to the two features resolved in the solid. The enhanced splitting, as well as the intensity redistribution, arises from coupling of the monomer ion states to the crystal environment via intermolecular screening processes.

Figure 11 and Table V indicate that the $O1s(NO_2)$ dimer shake-up transition is a relatively pure singly excited HOMO → LUMO excitation localized on the ionic part of the dimer: an intramolecular $D^+ \rightarrow A^-$ charge-transfer transition as found in the monomer. As observed experimentally, the relative $O1s$ shake-up intensity in the dimer is distinctly greater than that calculated for the monomer. In line with the above discussion of the monomer, the absolute value of the satellite intensity remains approximately a factor of 2 less than experiment. Again, considerable shake-up intensity is gained through strong positive interference with the ground state. The absence of strong intermolecular orbital mixing in the dimer supports our previous rationalization as to the similarity between the $O1s(NO_2)$ vapor and condensed phase spectra.[14]
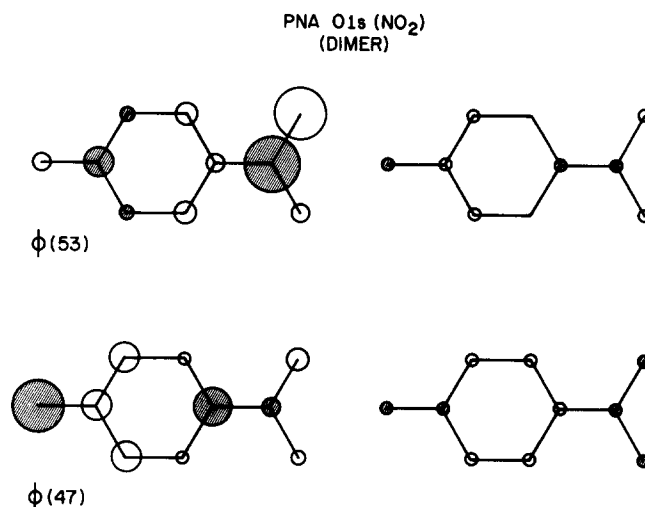
PNA O1s ($NO_2$)
(DIMER)



φ(53)

φ(47)

FIG. 11. The PNA $O1s(NO_2)$ dimer orbitals of interest.

## 2-Amino-6-nitronaphthalene (2,6-ANN)

Table VI compares the calculated lower-lying singlet $\pi^* \leftarrow \pi$ excitations of neutral 2,6-ANN with the experimental results of Pearson.[61] The relevant molecular orbitals used to address intramolecular charge-transfer behavior of the various excitations in the neutral and ionic species are given in Fig. 12. Table VI shows that the correlation of the calculated singlet transition energies versus the experimental values is quite good if it is assumed the weak $4\ {}^1A\ '(\pi^* \leftarrow \pi)$ and $5\ {}^1A\ '(\pi^* \leftarrow \pi)$ excitations lie under the more intense $3\ {}^1A\ '(\pi^* \leftarrow \pi)$ and $6\ {}^1A\ '(\pi^* \leftarrow \pi)$ transitions. Pearson has, in fact, noted an asymmetry in the third absorption band.[61] Also, the computed oscillator strengths and solvent shifts are in relative accord with experiment.

It is interesting at this point to compare selected properties of 2,6-ANN with those of PNA and 1,4-ANN: the *apparent* PNA analog. 1,4-ANN exhibits an experimental and computational (CNDO/S) absorption spectrum partially parallelling PNA [i.e., a single intense long wavelength tran-

TABLE V. Computational results on the PNA $O1s(NO_2)$ dimer core hole.

| Contributing determinants | | | |
|---|---|---|---|
| Order | Determinant(DET) | $\langle \Psi_{b \rightarrow c}^{a \rightarrow d}(I) | \Psi_{GS}(N) \rangle$ | $E^{DET}(eV)$ |
| 1 | (0,0 ‖ 0,0) | 0.796 490 | 0.0 |
| 2 | (0,47 ‖ 53,0) | $-$ 0.184 004 | 3.82 |

| | Final-state distribution | | |
|---|---|---|---|
| State | (0,0 ‖ 0,0) CI coefficient | $|\langle \Psi_F(I) | \Psi_{GS}(N) \rangle|^2(\%)$ | $E^F(eV)$ |
| 1 | 0.980 97 | 57.71 | 0.0 |
| 2 | $-$ 0.146 76 | 8.22 | 2.77 |

| State | Wave function (CI vector) |
|---|---|
| 1 | 0.980 97 (0,0 ‖ 0,0) + ⋯ |
| 2 | $-$ 0.146 76 (0,0 ‖ 0,0) + 0.875 95 (0,47 ‖ 53,0) + ⋯ |

TABLE VI. The low-lying $\pi^* \leftarrow \pi$ singlet excitations and related properties of PNA, 1,4-ANN, and 2,6-ANN. The theoretical results were obtained according to the CNDO/S method $[\beta(O) = -45.0$ eV] with configuration interaction between the 60 lowest-energy singly excited configurations using the Nishimoto–Mataga integral approximation. Experimental excitation energies were collected from various sources: vapor phase (V)—Teng and Garito (Ref. 60), cyclohexane solution (C)—Pearson (Ref. 61), ethanol solution (E)—Pearson (Ref. 61), and condensed phase EPA (EPA)—Khalil and McGlynn (Ref. 62). The experimental oscillator strengths were estimated from the extinction coefficients $\epsilon_{MAX}(\nu)$ according to the relationship $f^*_{EXP} = \xi \, \Delta\nu_{1/2} \, \epsilon_{MAX}(\nu)$ where $\xi = 4.319 \times 10^{-9}$ M cm$^{-2}$ and $\Delta\nu_{1/2} = 5.0 \times 10^3$ cm$^{-1}$. It has been our experience when applying the CNDO/S approximation to polar compounds bearing the nitro group that the ground state dipole moment $(\mu_g)$ is calculated $\sim$2.0 D higher than observed. We attribute this to an overestimation of ground state charge transfer character between the nitrogen and oxygen atoms. Since this factor appears in the excited states as well, ground and excited state dipole moment differences are expected to be relatively accurate. $\Delta\mu_{e-g} = 10.12$ D for the first calculated PNA excited state, compared to the experimental value of 10.3 D—Ledger and Suppan (Ref. 63).

| Character | $^1E_T$(eV) | $E_{EXP}$(eV) | $f^*_{EXP}$ | $f(S_n \leftarrow S_0)$ | $\mu_e$(D) | Wave function |
|---|---|---|---|---|---|---|
| | | | PNA($\mu_g = 7.72$ D) | | | |
| 1 $^1A_1$ | 4.33 | $\sim$4.25(V),3.82(C),3.30 (E) | 0.32(E,EPA) | 0.5101 | 17.84 | $-$ 0.980 (26,27) $-$ 0.105 (25,28) $+$ ... |
| 1 $^1B_2$ | 4.42 | 4.13(EPA) | 0.032(EPA) | 0.0004 | 10.21 | 0.718 (25,27) $-$ 0.625 (26,28) $+$ ... |
| 3 $^1B_2$ | 5.39 | 5.7(V),5.43(C),5.41(E) | 0.13(E) | 0.0925 | 16.42 | $-$ 0.688 (25,27) $-$ 0.611 (26,28) $+$ ... |
| 4 $^1A_1$ | 5.85 | ... | ... | 0.0058 | 11.46 | $-$ 0.898 (26,29) $+$ 0.403 (25,28) $+$ ... |
| 5 $^1B_2$ | 6.26 | ... | ... | 0.0754 | 2.72 | 0.878 (24,27) $+$ 0.438 (25,29) $+$ ... |
| 6 $^1A_1$ | 6.65 | $>$6.20(EPA) | $>$0.32(EPA) | 0.9245 | 7.91 | $-$ 0.380 (26,29) $-$ 0.890 (25,28) $+$ ... |
| 7 $^1B_2$ | 6.69 | ... | ... | 0.9112 | 7.48 | 0.411 (24,27) $-$ 0.744 (25,29) $+$ ... |
| | | | 1,4-ANN ($\mu_g = 7.21$ D) | | | |
| 1 $^1A'$ | 3.38 | 3.29(C),2.88(E) | 0.26(C) | 0.4182 | 14.84 | $-$ 0.974 (35,36) $+$ 0.129 (35,37) $+$ ... |
| 2 $^1A'$ | 3.89 | ... | ... | 0.0012 | 7.71 | $-$ 0.646 (34,36) $-$ 0.689 (35,38) $+$ ... |
| 3 $^1A'$ | 4.59 | ... | ... | 0.0123 | 10.45 | $-$ 0.930 (35,37) $-$ 0.166 (32,36) $+$ ... |
| 4 $^1A'$ | 4.89 | 4.94(C),4.76(E) | 0.35(C) | 0.4677 | 14.16 | 0.713 (34,36) $+$ 0.549 (35,38) $+$ ... |
| 5 $^1A'$ | 5.16 | ... | ... | 0.1783 | 13.91 | 0.949 (32,36) $-$ 0.169 (35,37) $+$ ... |
| | | | 2,6-ANN ($\mu_g = 8.15$ D) | | | |
| 1 $^1A'$ | 3.55 | 3.40(C),3.06(E) | 0.29(C) | 0.2011 | 15.61 | 0.841 (35,36) $+$ 0.282 (35,37) $+$ ... |
| 2 $^1A'$ | 3.88 | 4.43(C),4.22(E) | 0.25(C) | 0.1705 | 12.84 | 0.483 (35,36) $-$ 0.552 (35,37) $+$ ... |
| 3 $^1A'$ | 4.70 | 4.81(C),4.81(E) | 0.37(C) | 0.8615 | 13.64 | 0.732 (35,37) $-$ 0.493 (34,36) $+$ ... |
| 4 $^1A'$ | 4.80 | ... | ... | 0.1127 | 17.66 | $-$ 0.511 (34,36) $-$ 0.550 (35,38) $+$ ... |
| 5 $^1A'$ | 5.41 | ... | ... | 0.1598 | 9.08 | 0.357 (35,38) $-$ 0.811 (35,39) $+$ ... |
| 6 $^1A'$ | 5.58 | 5.49(C),5.30(E) | 0.70(C) | 0.9345 | 10.34 | $-$ 0.539 (35,38) $+$ 0.651 (34,37) $+$ ... |

sition (see Table VI), and based on the relative resonance structures which can be constructed one might expect that the $D^+ \rightarrow A^-$ charge-transfer state of 2,6-ANN would absorb at longer wavelengths and exhibit a greater solvent sensitivity than the corresponding 1,4-ANN and PNA excitation. Although 2,6-ANN and 1,4-ANN absorb at longer wavelengths than PNA as anticipated based on the relative energy levels of the phenyl and naphthalene frameworks (see below), 2,6-ANN shows a slightly *smaller* solvent sensitivity than either PNA or 1,4-ANN. This is in accord with the calculated dipole moment differences $(\Delta\mu_{e-g})$ given in Table VI. This can be rationalized by noting that in PNA the HOMO level is largely localized on the –NH$_2$ group, whereas in 2,6-ANN *and* 1,4-ANN this donor group $\pi$ level is distributed approximately evenly among three lower binding energy orbitals localized mainly on the naphthalene moiety. Although the –NH$_2$ group is still classified in 2,6-ANN and 1,4-ANN as a strong $\pi$-electron donor based on calculated ground state charge densities, such donor character is not reflected directly in the long wavelength excitation spectra. Charge-transfer excitation from the amino group in 2,6-ANN is $< -0.100e$ in all excitations given in Table VI. Both low-lying intense 1,4-ANN singlet transitions reflect – NH$_2$ group charge transfer of $< -0.030e$ according to our calculations. The lowest energy $\pi^* \leftarrow \pi$ singlet transitions of 2,6-ANN and 1,4-ANN remain classified as charge-transfer excitations, however; but of Ar→NO$_2$ character. In addi-
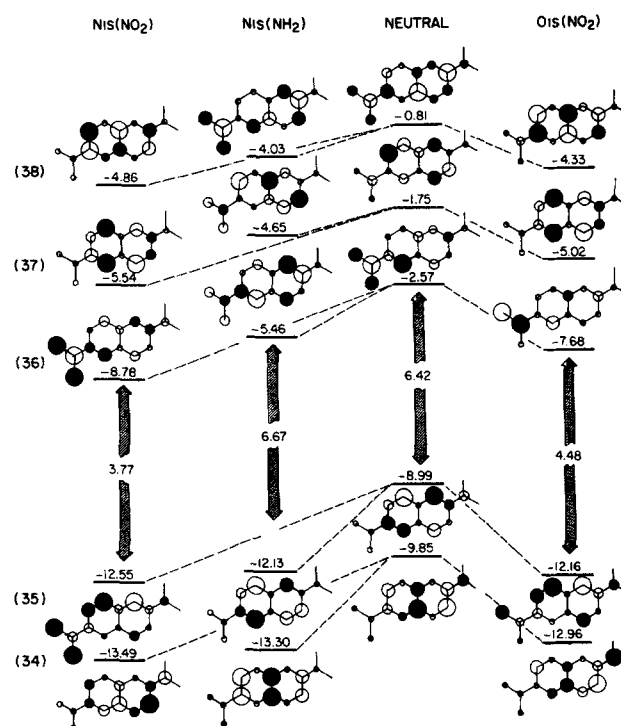


FIG. 12. The occupied and virtual orbitals of interest obtained from the neutral and indicated $(Z + 1)$—computations on 2,6-ANN using the CNDO/S method with Nishimoto–Mataga integrals. All energies are given in eV.

tion, the lowest excited state Ar→NO$_2$ charge-transfer character is considerably reduced in 2,6-ANN and 1,4-ANN relative to PNA (0.349, 0.401, and 0.614$e$, respectively). The origin of the large $\Delta\mu_{e-g}$ values exhibited by 2,6-ANN and 1,4-ANN therefore appears to be a relatively small charge transfer over a greater distance. This is contrasted in PNA where ~0.6$e$ is given a shorter displacement.

Further evidence that the CNDO/S method adequately reflects the nature of the electronic structure of PNA, 1,4-ANN, and 2,6-ANN is given in Fig. 13 where the Koopmans' theorem ionization potentials (I.P.) are shown to adequately correlate with the relative splittings observed in the gas phase photoelectron spectra. In comparison to the unsubstituted phenyl and naphthalene moieties it is expected that –NH$_2$ group substitution would destabilize the low-lying $\pi$ orbitals depending on the magnitude of the amino nitrogen AO coefficient, whereas –NO$_2$ group character is



FIG. 13. A comparison of the experimental vapor phase UPS spectra of PNA [Khalil and co-workers (Ref. 64)], and 1,4-ANN and 2,6-ANN [Distefano *et al.* (Ref. 5)] with the CNDO/S Koopmans' theorem ionization potentials (Nishimoto–Mataga integrals). All computed energies are relative to the PNA HOMO value which was referenced to the experimental feature of lowest energy.

probed from the LUMO properties, or the higher-lying occupied levels. On going from benzene to PNA the first I.P. is reduced from 9.25[65]→8.60 eV[64] ($\Delta E = 0.65$ eV), whereas on going from naphthalene to 2,6-ANN and 1,4-ANN the first I.P.'s are only shifted from 8.15[65]→8.06[5] and 8.05 eV[5] ($\Delta E = 0.09$ and 0.10 eV, respectively). Such relative behavior is reflected in the computational comparisons given in Fig. 13. Therefore, the "similarity" between the neutral molecule absorption spectra of PNA and 1,4-ANN appears somewhat fortuitous based on our computational results. Differences in the details of the final-state CI account for the observed variations in the singlet absorption spectra on going from 2,6-ANN to 1,4-ANN.

Figure 14 and Table VII indicates that five final-states derived from 12 initial configurations below 5.0 eV contribute to the N1$s$(NO$_2$) monomer ionization spectrum of 2,6-ANN in the energy range of interest. Due to their energetic proximity the final-states sum to give a broad peak structure as observed experimentally. As observed in the solid state the theoretical N1$s$(NO$_2$) monomer species has already developed a ground state with significantly less ionization intensity than the sum of the more closely spaced higher-energy features. The very low-lying double-substitutions arising from the HOMO level and the density of initial configurations lead to a final-state spectrum rich in correlation effects: the ground state being the only final state which retains a > 50% single configuration character.

Electron density difference plots between the three lowest energy shake-up states of largest intensity and the ground state of the ion are given in Figs. 15(a)–15(c). State #2 [Figure 15(a)] describes strong charge transfer mainly out of the aromatic ring system onto the –NO$_2$ group. The second shake-up transition leading to the state #3 [Figure 15(b)] can be viewed as a "charge oscillation" basically confined to the ring system, whereas excitation to state #4 essentially involves a charge rearrangement within the NO$_2$ group.

The large relative depletion of intensity from the ionic ground state (0,0 ∥ 0,0) by CI can be rationalized by recognizing that such effects are to be expected whenever the SCF configuration poorly describes charge relaxation, and whenever suitable low-lying excited states are available to screen the core hole. Mixing occurs between the SCF ionic ground state, which has large overlap with the neutral molecule occupied orbitals, and appropriate low-lying excited configurations which have small neutral molecule overlap leading to a final state with reduced intensity. Corresponding interactions were calculated for PNA N1$s$(NO$_2$) monomer and dimer ionizations (Tables II and IV). The effect is relatively large in the 2,6-ANN monomer due to the close spacing of the occupied and virtual levels in the N1$s$(NO$_2$) ion. Such destructive interference is almost complete in the case of PNA N1$s$(NO$_2$) dimer ionization, as CI leads to a lowest-energy state having an ~4.0% intensity. As shown below and in Fig. 14 the effect appears greater still for N1$s$(NO$_2$) ionization of 2,6-ANN in the solid.

As reflected by the relative HOMO/LUMO spacings, O1$s$(NO$_2$) ionization of 2,6-ANN leads to considerably less correlation mixing than found in the N1$s$(NO$_2$) ion, although final-state interactions are greater than for O1$s$(NO$_2$) ioniza-

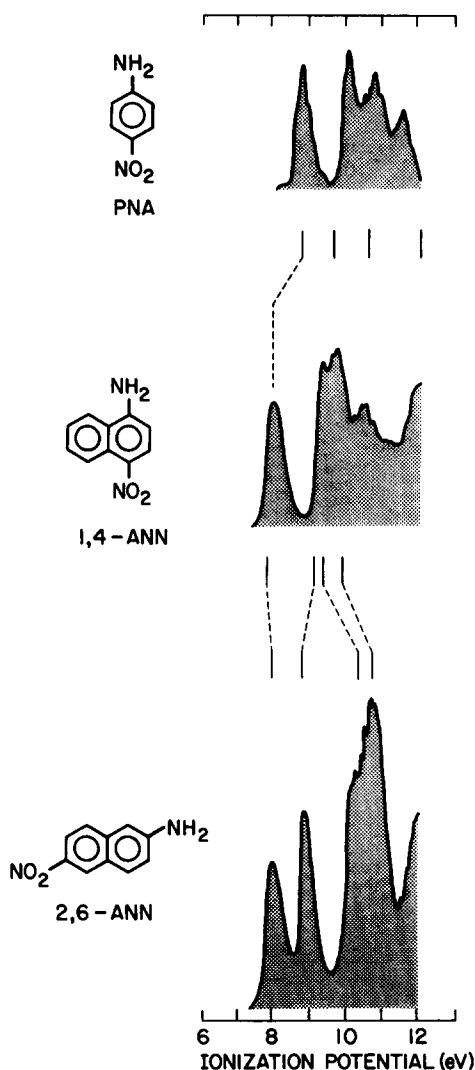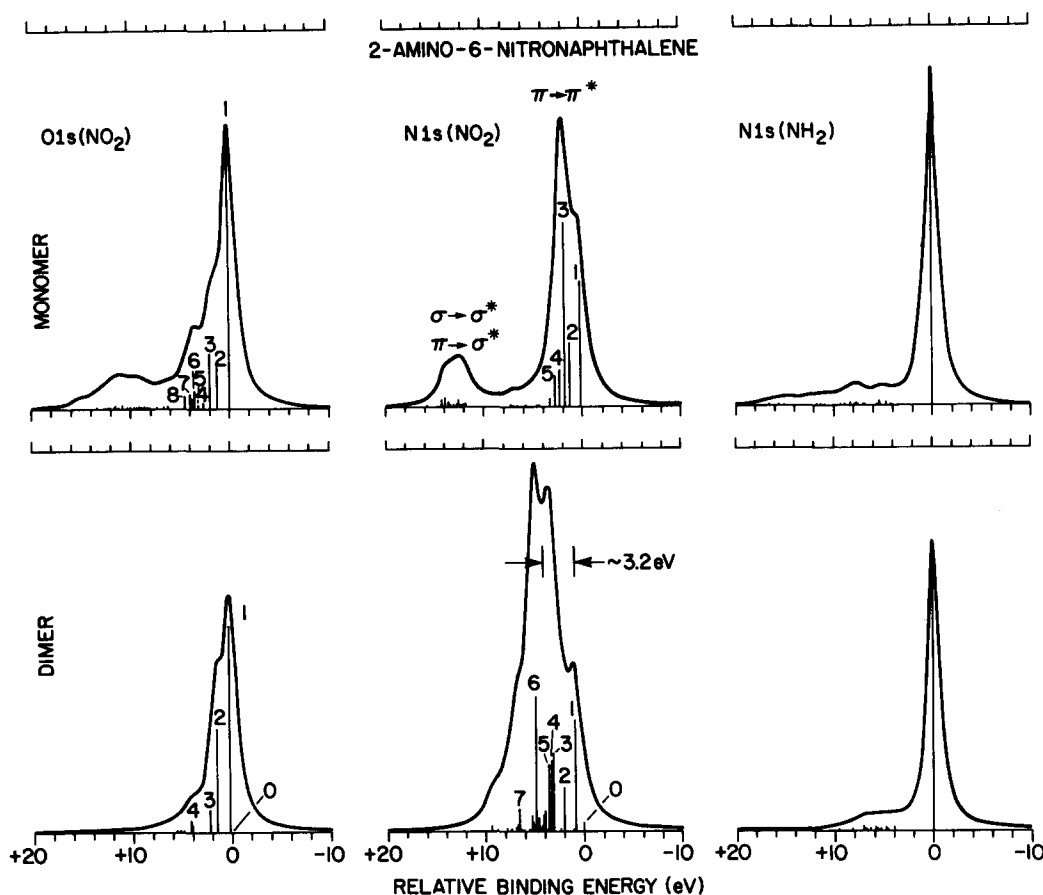FIG. 14. The theoretical monomer and dimer N1s(NO₂), O1s(NO₂), and N1s(NH₂) core-hole spectra of 2,6-ANN obtained using correlated ion states.

tion of PNA (Fig. 14 and Table VIII). A comparison of the calculated and experimental O1s(NO₂) and N1s(NO₂) vapor phase spectra of 2,6-ANN is given in Fig. 16 where the relative N1s binding energies were obtained according to Eq. (2).

Figures 14 and 17, and Table IX indicate that the 2,6-ANN N1s(NO₂) dimer spectrum is more complex than the monomer or dimer ionizations considered above. The final-state spectrum, however, clearly yields a relatively weak well-resolved feature on the low-binding energy side of the main component as observed experimentally. The N1s(NO₂) dimer orbital mixing effects reflect the relative –NH₂ π-orbital delocalization and the energy of the HOMO level in the neutral fragment. This situation yields an ionized dimer HOMO/LUMO spacing of 1.68 eV, compared to $\lesssim 3.0$ eV in the PNA dimer, which provides an abundance of low-lying doubly excited configurations. Final-state #2 is the only state which maintains >50% single configuration character. All others are strongly correlated, consisting primarily of $D^+{\rightarrow}A^-$ and $Ar{\rightarrow}A^-$ intramolecular charge-transfer configurations. In addition to the large density of low-lying excitations, there are at least four excited configurations having a large overlap with the neutral dimer ground state determinant.

It should be emphasized that final-state #1 in the N1s(NO₂) ionized monomer essentially corresponds to the final-state labeled #1 in the dimer, although the dimer model has lower-lying levels. The monomer final-state #1 is a destructive combination of the ground and doubly excited

HOMO →LUMO configurations which yield a reduced intensity, whereas final-state #1 in the dimer is a constructive coupling of the ground and singly excited HOMO →LUMO levels with a destructive component due to the doubly excited (68,68 || 71,71) configuration. The (68,68 ||71,71) dimer and (35,35||36,36) monomer configurations are similar in that each are excitations "localized" on the –NO₂ group. The dimer final-state #1 is therefore pushed (pulled) to lower relative energy than in the monomer by enhanced CI. The final-state denoted as #0 in Fig. 14 arises from a large destructive interference between the ground configuration and low-lying intermolecular charge-transfer excitations, and carries approximately zero intensity.

In order to check the sensitivity of the final-state distribution on the geometry chosen to reflect the solid state interactions we performed comparison calculations on the N1s(NO₂) spectrum of a "twisted" dimer formed by rotating the neutral part 45° around the axis of the H₂ N–C bond while keeping the –N⁺O₂/H₂N–nitrogen–nitrogen intermolecular bondlength at 3.0 Å. Figure 18 indicates that while some of the final states are reordered in energy and intensity, the twisted dimer yields an ionization pattern parallelling the planar model.

Figure 19 and Table X shows that the O1s(NO₂) ionization of 2,6-ANN in the solid compares favorably with the monomer situation. As in the case of PNA, negligible intermolecular orbital mixing is induced by the O1s(NO₂) core hole. Although the O1s(NO₂) dimer has a HOMO/LUMO

TABLE VII. (A) Properties of the determinants contributing to the 2,6-ANN N1s(NO$_2$) monomer spectrum, and the final-state energy and intensity distributions; (B) selected final-state wave functions entering into the interpretation of the 2,6-ANN N1s(NO$_2$) monomer spectrum.

(A)

| | | Contributing determinants | |
|---|---|---|---|
| Order | Determinant(DET) | $\langle \Psi_{b \to c}^{a \to d}(I)| \Psi_{GS}(N)\rangle$ | $E^{DET}(eV)$ |
| 1 | (0,0 ‖ 0,0) | 0.5818 | 0.00 |
| 2 | (0,34 ‖ 36,0) | 0.0488 | 1.71 |
| 3 | (35,35 ‖ 36,36) | 0.2374 | 2.10 |
| 4 | (0,35 ‖ 36,0) | 0.3717 | 2.21 |
| 5 | (0,33 ‖ 36,0) | − 0.0731 | 3.05 |
| 6 | (34,35 ‖ 36,36) | 0.0312 | 3.18 |
| 7 | (0,35 ‖ 37,0) | − 0.0061 | 3.61 |
| 8 | (0,32 ‖ 36,0) | 0.0455 | 3.62 |
| 9 | (0,35) ‖ 38,0) | 0.0403 | 4.07 |
| 10 | (0,34 ‖ 37,0) | − 0.0139 | 4.39 |
| 11 | (35,35 ‖ 36,37) | − 0.0039 | 4.60 |
| 12 | (35,35 ‖ 36,38) | 0.0258 | 4.65 |

| | | Final-state distribution | |
|---|---|---|---|
| State | (0,0 ‖ 0,0) CI coefficient | $|\langle \Psi_F(I)| \Psi_{GS}(N)\rangle|^2$(Rel.) | $E^F(eV)$ |
| 1 | − 0.8192 | 100.0 | 0.00 |
| 2 | 0.1855 | 51.0 | 1.11 |
| 3 | − 0.2768 | 144.9 | 1.65 |
| 4 | 0.0313 | 29.8 | 2.18 |
| 5 | − 0.0421 | 25.2 | 2.66 |

(B)

| State | Wave function (CI vector) |
|---|---|
| 1 | − 0.8192 (0,0 ‖ 0,0) + 0.4498 (35,35 ‖ 36,36) + ⋯ |
| 2 | 0.1855 (0,0 ‖ 0,0) − 0.6578 (0,34 ‖ 36,0) + 0.3622 (0,35 ‖ 36,0) − 0.3836 (34,35 ‖ 36,36) + 0.2685 (35,35 ‖ 36,36) + ⋯ |
| 3 | − 0.2768 (0,0 ‖ 0,0) − 0.3479 (0,34 ‖ 36,0) − 0.3531 (35,35 ‖ 36,36) − 0.4968 (0,35 ‖ 36,0) − 0.2554 (0,33 ‖ 36,0) − 0.3223(34,35 ‖ 36,36) + ⋯ |
| 4 | 0.0313 (0,0 ‖ 0,0) + 0.2689 (0,35 ‖ 36,0) − 0.6104 (0,33 ‖ 36,0) − 0.2656(0,35 ‖ 37,0) + 0.2363(35,35 ‖ 36,36) − 0.4066(33,35 ‖ 36,36) + ⋯ |
| 5 | − 0.0421 (0,0 ‖ 0,0) − 0.2027 (35,35 ‖ 36,36) − 0.3555 (0,35 ‖ 37,0) − 0.3230(0,32 ‖ 36,0) − 0.3898(35,35 ‖ 36,37) + 0.2038(35,35 ‖ 36,38) + ⋯ |
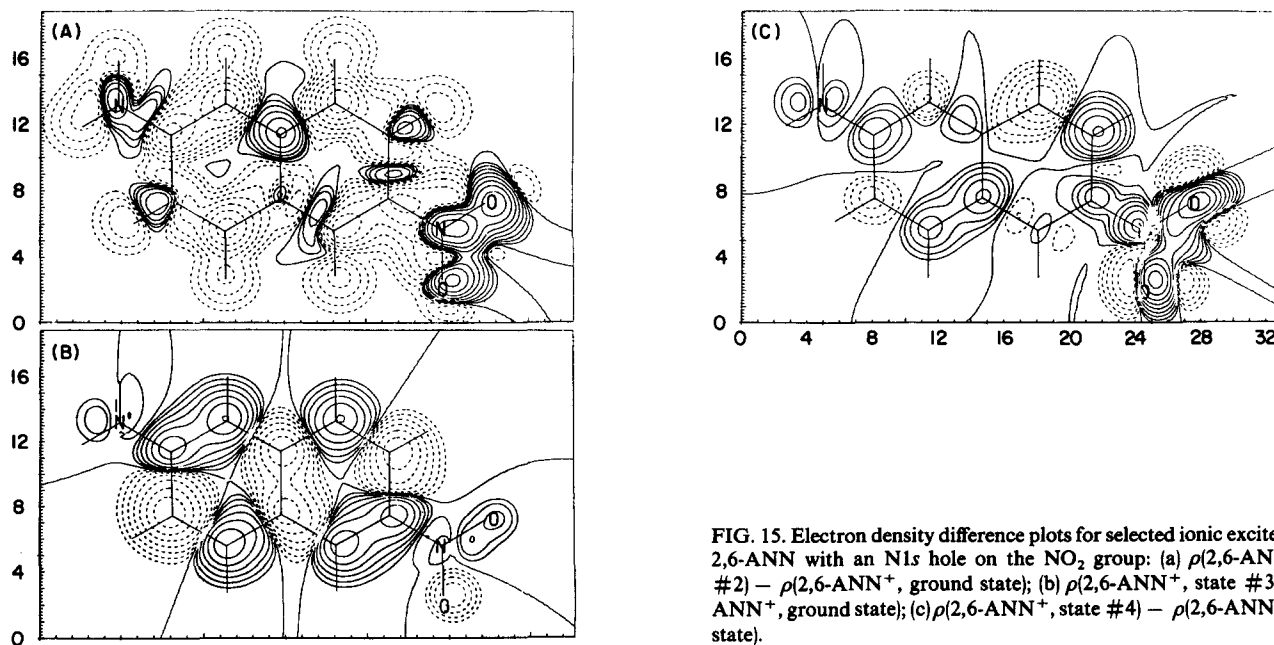


FIG. 15. Electron density difference plots for selected ionic excited states of 2,6-ANN with an N1s hole on the NO$_2$ group: (a) $\rho$(2,6-ANN$^+$, state #2) − $\rho$(2,6-ANN$^+$, ground state); (b) $\rho$(2,6-ANN$^+$, state #3) − $\rho$(2,6-ANN$^+$, ground state); (c)$\rho$(2,6-ANN$^+$, state #4) − $\rho$(2,6-ANN$^+$, ground state).

TABLE VIII. (A) Properties of the determinants contributing to the 2,6-ANN $O1s(NO_2)$ monomer spectrum, and the final-state energy and intensity distributions; (B) selected final-state wave functions entering into the interpretation of the 2,6-ANN $O1s(NO_2)$ monomer spectrum.

(A)

| | Contributing determinants | | |
|---|---|---|---|
| Order | Determinant(DET) | $\langle \Psi_{b \to c}^{a \to d}(\mathrm{I})|\Psi_{GS}(\mathrm{N})\rangle$ | $E^{DET}(eV)$ |
| 1 | (0,0 ‖ 0,0) | 0.7125 | 0.00 |
| 2 | (0,35 ‖ 36,0) | 0.2215 | 2.16 |
| 3 | (0,34 ‖ 36,0) | 0.0875 | 2.41 |
| 4 | (0,33 ‖ 36,0) | 0.0604 | 3.50 |
| 5 | (0,35 ‖ 37,0) | 0.0010 | 3.79 |
| 6 | (0,32 ‖ 36,0) | 0.0713 | 4.27 |
| 7 | (35,35 ‖ 36,37) | 0.0004 | 5.52 |
| 8 | (35,35 ‖ 36,36) | 0.0689 | 5.64 |
| 9 | (34,35 ‖ 36,36) | 0.0272 | 6.44 |
| 10 | (32,35 ‖ 36,36) | 0.0021 | 7.98 |

| | Final-state distribution | | |
|---|---|---|---|
| State | (0,0 ‖ 0,0) CI coefficient | $|\langle \Psi_F(\mathrm{I})|\Psi_{GS}(\mathrm{N})\rangle|^2(\mathrm{Rel.})$ | $E^F(eV)$ |
| 1 | − 0.8845 | 0.3178 | 0.00 |
| 2 | − 0.1716 | 0.0509 | 1.32 |
| 3 | − 0.1507 | 0.0657 | 2.04 |
| 4 | 0.0288 | 0.0074 | 2.72 |
| 5 | − 0.1051 | 0.0054 | 3.20 |
| 6 | 0.0561 | 0.0262 | 3.60 |
| 7 | − 0.0715 | 0.0134 | 3.75 |
| 8 | − 0.0640 | 0.0177 | 4.01 |

(B)

| State | Wave function (CI vector) |
|---|---|
| 1 | − 0.8845 (0,0 ‖ 0,0) + 0.1530 (0,35 ‖ 36,0) + 0.2059 (35,35 ‖ 36,36) + 0.1212 (32,35 ‖ 36,36) + ⋯ |
| 2 | − 0.6268 (0,35 ‖ 36,0) + 0.4966 (0,34 ‖ 36,0) + 0.3009 (35,35 ‖ 36,36) + ⋯ |
| 3 | − 0.4297 (0,35 ‖ 36,0) − 0.6141 (0,34 ‖ 36,0) + 0.2019 (0,33 ‖ 36,0) − 0.3073 (34,35 ‖ 36,36) + ⋯ |
| 4 | 0.6740 (0,33 ‖ 36,0) − 0.2417 (0,35 ‖ 37,0) + 0.2638 (35,35 ‖ 36,37) + ⋯ |
| 5 | − 0.4761 (0,35 ‖ 37,0) − 0.3538 (0,35 ‖ 38,0) + 0.3030 (0,32 ‖ 36,0) + 0.2128 (35,35 ‖ 36,37) − 0.2651 (35,35 ‖ 36,36) + ⋯ |
| 6 | − 0.3368 (35,35 ‖ 36,37) − 0.3546 (35,35 ‖ 36,39) + ⋯ |
| 7 | − 0.2506 (0,35 ‖ 38,0) − 0.3792 (0,32 ‖ 36,0) + 0.5528 (0,34 ‖ 37,0) − 0.2155 (34,35 ‖ 36,37) + ⋯ |
| 8 | − 0.4096 (0,35 ‖ 37,0) + 0.4091 (0,35 ‖ 38,0) + 0.3315 (0,35 ‖ 39,0) + ⋯ |

gap of only ∼2.0 eV, the HOMO level is "completely" localized on the neutral fragment and does not enter into our interpretation of the ionization spectrum.

## 1-Amino-4-nitronaphthalene (1,4-ANN)

Although we have not determined a crystal structure for 1,4-ANN, or performed doubly excited state computations on the monomer and assumed dimer equivalent-core ions, it is nevertheless useful to note trends in the experimental spectra and to compare these trends with various one-electron properties (Table XI). First, the vapor phase core-hole spectra of PNA, 2,6-ANN, and 1,4-ANN "essentially"

indicate broad single peak $N1s(NO_2)$ structures. This is in accord with the similarities in the equivalent-core singly excited HOMO →LUMO excitation energies. Experiment also indicates that the $O1s(NO_2)$ vapor phase shake-up energies are in the order PNA > 1,4-ANN > 2,6-ANN (see Table I). This ordering again parallels the relative equivalent-core singly excited HOMO →LUMO transition energies. Although detailed correlations between shake-up intensities cannot be drawn due to the single peak nature of the spectra, the equivalent-core SCF results suggest a significantly greater intramolecular orbital mixing for both $O1s(NO_2)$ and $N1s(NO_2)$ ionization of 1,4-ANN. It is interesting to note that the ordering of the 2,6-ANN and 1,4-ANN neutral molecule excitations (experimental *and* calculated) are reversed
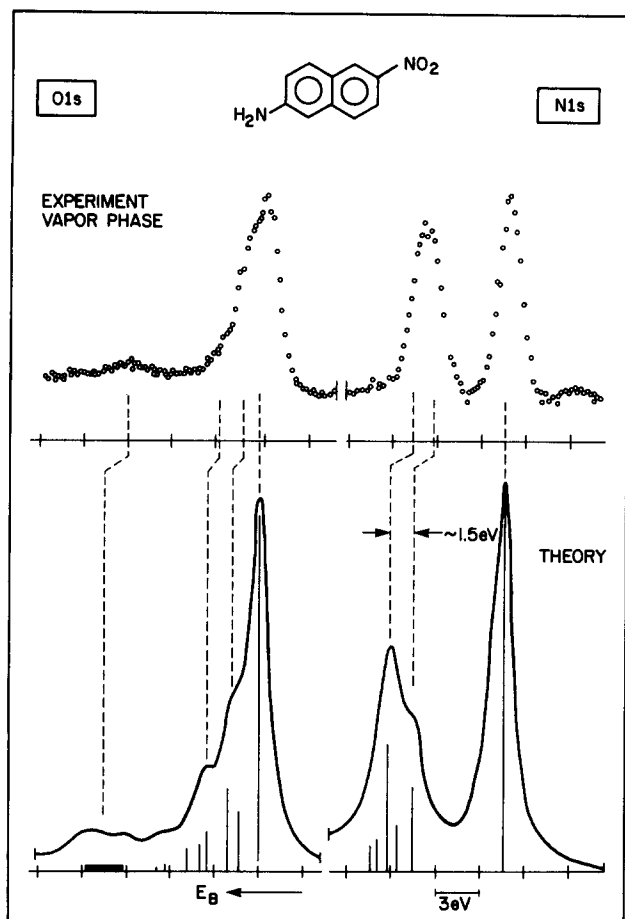
FIG. 16. Comparison of the 2,6-ANN monomer final ion-state distributions with the experimental vapor phase spectra.
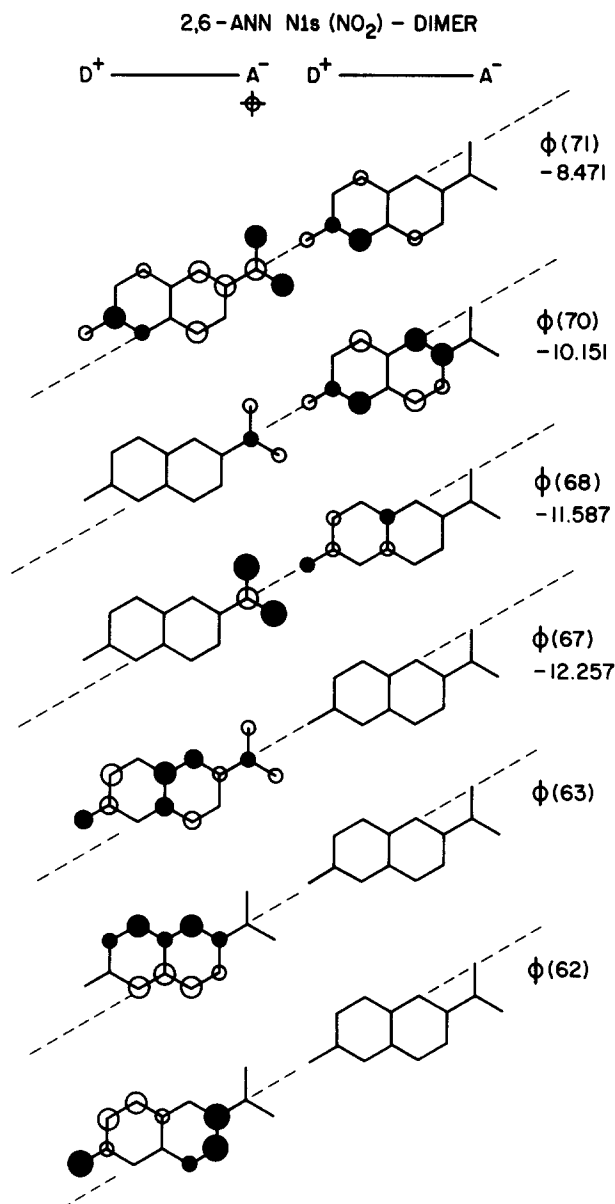


FIG. 17. The 2,6-ANN N1s(NO₂) dimer orbitals of interest. All energies are given in eV. The orbital lobes are drawn proportional to the LCAO coefficients and viewed from above the molecular plane.

relative to those of the equivalent-core species and the experimental O1s shake-up features (see Table XI). This reversal of energy levels on going to the core-ionized species can be rationalized by noting that the overlap factor $\langle j'(1)|i(N)\rangle$ for both N1s(NO₂) and O1s ionization is significantly greater for 1,4-ANN than 2,6-ANN. Due to the apparent enhanced overlap attributed to core-hole induced orbital mixing in 1,4-ANN, selective HOMO/LUMO Coulomb interactions are inhibited.

Further comparison of the experimental spectra (Figs. 1–3) reveals that on going from the vapor phase to the solid state the N1s(NO₂) features of PNA, 2,6-ANN, and 1,4-ANN are considerably split, whereas the O1s(NO₂) ionizations of PNA and 2,6-ANN appear essentially unperturbed. The O1s(NO₂) ionization of 1,4-ANN, however, exhibits not only a moderately enhanced splitting on going to the solid (~1.9 to ~2.4 eV); but an apparent *decrease* in shake-up intensity as well (from ~50% in the vapor phase to ~30% in the solid). As discussed above, the relative difference in the N1s(NO₂) ionization of PNA is attributed partly to intermolecular orbital mixing between the HOMO level of the ionic part of the dimer with an underlying neutral part orbital localized on the –NH₂ group. O1s(NO₂) ionization was indicated to pull the –NH₂ localized neutral fragment sufficiently below the ionic HOMO level so as to render interaction

unfavorable. Also as noted above, the higher-lying –NH₂ π orbital (the HOMO level in PNA) becomes delocalized in 2,6-ANN and 1,4-ANN and contributes to three moderately spaced levels localized on the naphthalene backbone. Taking the neutral moiety levels with the largest –NH₂ π-orbital contributions as potential sources of intermolecular interaction suggests the orbital correlation diagram given in Fig. 20. Therefore, assuming reasonable electrostatic displacements of the neutral part due to core ionization,[14] Fig. 20 yields only four situations where significant intermolecular interaction with the HOMO level of the ionic part is expected. The four conditions of "orbital proximity" identified in Fig. 20 are derived from ionizations where the apparent greatest vapor phase to solid state shifts are experimentally observed. As indicated above, these relationships have been computationally verified for PNA and 2,6-ANN.

TABLE IX. (A) Properties of the determinants contributing to the 2,6-ANN N1s(NO₂) dimer spectrum, and the final-state energy and intensity distributions; (B) selected final-state wave functions entering into the interpretation of the 2,6-ANN N1s(NO₂) dimer spectrum.

(A)

**Contributing determinants**

| Order | Determinant(DET) | $\langle \Psi^{a \rightarrow d}_{b \rightarrow c}(\mathrm{I}) \vert \Psi_{GS}(\mathrm{N}) \rangle$ | $E^{DET}(eV)$ |
|---|---|---|---|
| 1 | (0,0 ‖ 0,0) | 0.4398 | 0.00 |
| 2 | (70,70 ‖ 71,71) | 0.1163 | 0.94 |
| 3 | (0,70 ‖ 71,0) | 0.2154 | 1.26 |
| 4 | (0,68 ‖ 71,0) | − 0.3254 | 1.34 |
| 5 | (68,70 ‖ 71,71) | − 0.1594 | 1.46 |
| 6 | (0,67 ‖ 71,0) | − 0.0727 | 1.62 |
| 7 | (69,70 ‖ 71,71) | − 0.1151 | 1.63 |
| 8 | (68,68 ‖ 71,71) | 0.2408 | 2.04 |
| 9 | (67,68 ‖ 71,71) | 0.0538 | 2.48 |
| 10 | (0,63 ‖ 71,0) | 0.0639 | 3.03 |
| 11 | (62,70 ‖ 71,71) | 0.0164 | 3.31 |
| 12 | (0,62 ‖ 71,0) | 0.0334 | 3.43 |
| 13 | (63,70 ‖ 71,71) | 0.0313 | 4.32 |

**Final-state distribution**

| State | (0,0 ‖ 0,0) CI coefficient | $\vert \langle \Psi_F(\mathrm{I}) \vert \Psi_{GS}(\mathrm{N}) \rangle \vert^2 (\text{Rel.})$ | $E^F(eV)$ |
|---|---|---|---|
| 0 | − 0.6245 | 100.0 | 0.00 |
| 1 | 0.5754 | 1318.6 | 0.99 |
| 2 | − 0.1252 | 523.2 | 2.14 |
| 3 | 0.1258 | 921.3 | 3.20 |
| 4 | − 0.1129 | 834.3 | 3.35 |
| 5 | 0.0779 | 754.3 | 3.56 |
| 6 | − 0.1174 | 1599.3 | 5.02 |
| 7 | 0.0361 | 267.9 | 6.64 |

(B)

| State | Wave function (CI vector) |
|---|---|
| 0 | − 0.6245 (0,0 ‖ 0,0) + 0.5057 (70,70 ‖ 71,71) − 0.3352 (0,70 ‖ 71,0) + 0.2983 (68,70 ‖ 71,71) − 0.2251 (69,70 ‖ 71,71) + ⋯ |
| 1 | 0.5754(0,0 ‖ 0,0) + 0.5065(0,70 ‖ 71,0) − 0.4344 (68,68 ‖ 71,71) + ⋯ |
| 2 | − 0.1252 (0,0 ‖ 0,0) − 0.7196 (0,67 ‖ 71,0) + 0.4268 (67,68 ‖ 71,71) + ⋯ |
| 3 | 0.1258 (0,0 ‖ 0,0) − 0.2998 (0,68 ‖ 71,0) + 0.2759 (63,70 ‖ 71,71) − 0.5348 (0,63 ‖ 71,0) + ⋯ |
| 4 | − 0.1008 (0,0 ‖ 0,0) + 0.5740 (63,70 ‖ 71,71) + 0.2161 (62,70 ‖ 71,71) + ⋯ |
| 5 | 0.0779 (0,0 ‖ 0,0) − 0.2327 (68,70 ‖ 71,71) − 0.2524 (0,68 ‖ 71,0) + 0.4493 (0,63 ‖ 71,0) − 0.4665 (0,62 ‖ 71,0) + ⋯ |



2,6-ANN
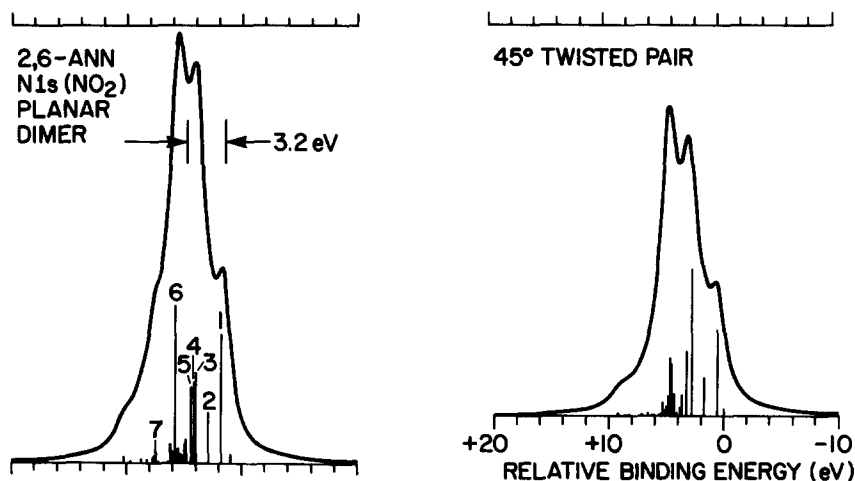N1s (NO₂)
PLANAR
DIMER ← 3.2 eV

45° TWISTED PAIR

FIG. 18. Comparison of the calculated 2,6-ANN N1s(NO₂) planar dimer spectrum with the corresponding distribution obtained by rotating the neutral part 45° as described in the text.
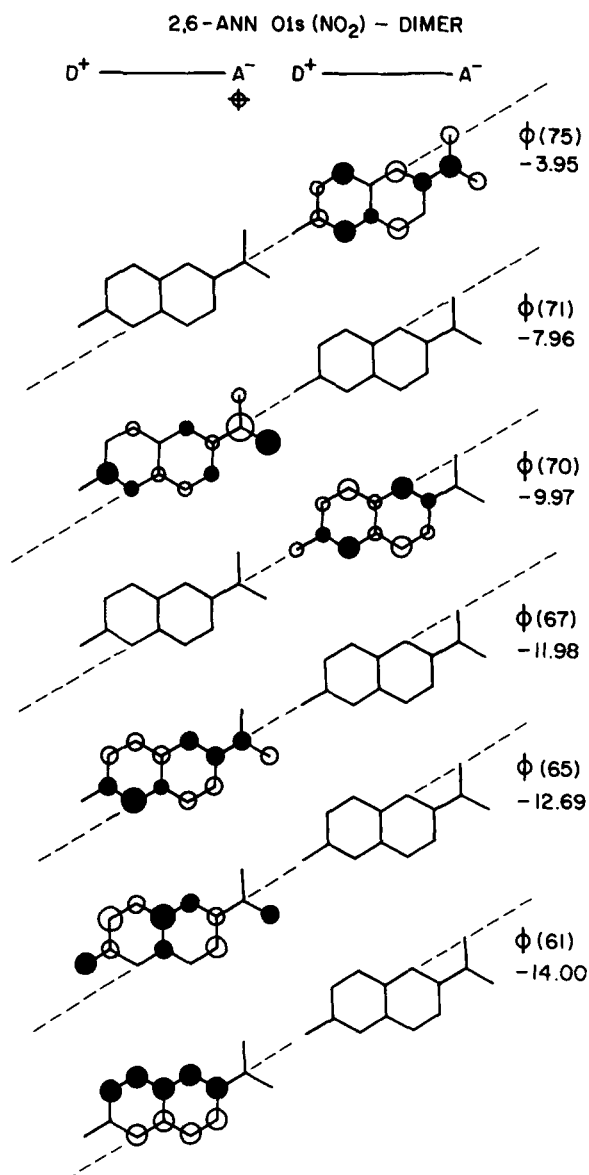
+20    +10    0    −10
RELATIVE BINDING ENERGY (eV)

2,6-ANN O1s (NO₂) − DIMER



FIG. 19. The 2,6-ANN O1s(NO₂) dimer orbitals of interest. All energies are in eV. The orbital lobes are drawn proportional to the LCAO coefficients and viewed from above the molecular plane.

## SUMMARY AND CONCLUSIONS

This study has presented new gas phase core-ionization spectra of 2-amino-6-nitronaphthalene (2,6-ANN) and 1-amino-4-nitronaphthalene (1,4-ANN). Comparison of the gas phase results with the complex solid-state spectra indicate significant intermolecular interactions as in the $D^+$–Ar–A⁻ model system $p$-nitroaniline (PNA). CNDO/S(CI) equivalent-core computations including up to doubly excited "singlet-coupled" substitutions were performed on the monomer and model dimer configurations which were shown to reflect the fundamental nature of the energy and intensity distributions observed in PNA and 2,6-ANN. Large correlation or many-body interactions, however, were found to yield final-state spectra which were generally not tractable in terms of singly excited configurations, although correlations were indicated between experimental trends and various one-electron properties. Differences in the mon-

omer to dimer final-state distributions were shown to be consistent with strong *intermolecular* core-hole induced orbital mixing. Also, we conclude that the similar N1s(NO₂) and O1s(NO₂) solid-state spectra exhibited by 1,4-ANN and PNA is somewhat fortuitous. Our results indicate that the electronic structure of 1,4-ANN, the PNA analog, has a closer correspondence to that of 2,6-ANN. It was rationalized that differences in the details of the intermolecular interactions resulted in similar final-state distributions.

We have not specifically addressed the issue that "weak" hydrogen-bonding interactions may actually be the source of the interesting vapor to condensed phase manifestations discussed in this work, although our results suggest otherwise. Based on our calculated electronic structures, and assuming a similar intermolecular pairing in 1,4-ANN as in PNA and 2,6-ANN, hydrogen-bonding interactions of the type suggested by Ågren and co-workers[25] would be expected to yield similar vapor phase to solid state perturbations for core ionization of 2,6-ANN and 1,4-ANN; a condition which is not verified experimentally. Our computations indicate that hydrogen-bonding induced selective HOMO/LUMO stabilization, which may be significant for the neutral species, would be largely destroyed in the ion due to HOMO/LUMO orbital mixing. N,N-dimethyl-$p$-nitroaniline (DMPNA) appears to be a case in point. Gas phase UPS spectra demonstrate that the HOMO level of PNA is *destabilized* by ~0.75 eV[64] due to dimethyl substitution at the amino nitrogen; yielding a condition approximating initial-state hydrogen-bonding between PNA molecules.[14] It is known, however, that DMPNA exhibits an N1s(NO₂) and
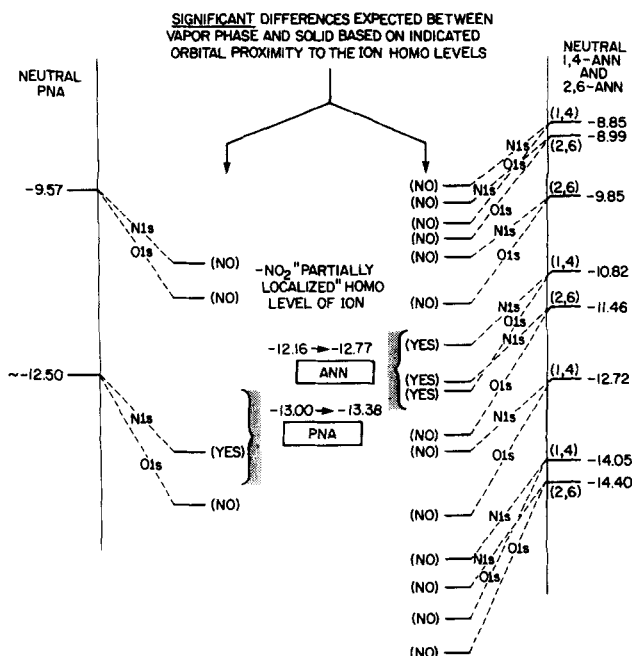


FIG. 20. Relative PNA, 2,6-ANN, and 1,4-ANN ion-state dimer correlation diagram emphasizing interactions between the HOMO level of the ions and various underlying –NH₂ localized neutral part orbitals. Energies are in electron volts. Mixing between the HOMO level of the neutral fragments with the LUMO level of the ions, which is strong for N1s(NO₂) PNA ionization and small or moderate for N1s(NO₂) 2,6-ANN ionization, is not considered.

TABLE X. (A) Properties of the determinants contributing to the 2,6-ANN $O1s(NO_2)$ dimer spectrum, and the final-state energy and intensity distributions; (B) selected final-state wave functions entering into the interpretation of the 2,6-ANN $O1s(NO_2)$ dimer spectrum.

**(A)**

Contributing determinants

| Order | Determinant(DET) | $\langle \Psi_{b\to c}^{a\to d}(I)|\Psi_{GS}(N)\rangle$ | $E^{DET}(eV)$ |
|---|---|---|---|
| 1 | (0,0 ‖ 0,0) | 0.7071 | 0.00 |
| 2 | (0,70 ‖ 71,0) | 0.0086 | 0.41 |
| 3 | (0,67 ‖ 71,0) | 0.2296 | 2.17 |
| 4 | (0,65 ‖ 71,0) | − 0.0846 | 2.37 |
| 5 | (67,70 ‖ 71,71) | 0.0028 | 3.37 |
| 6 | (0,61 ‖ 71,0) | 0.0691 | 3.47 |
| 7 | (0,70 ‖ 75,0) | 0.0163 | 3.56 |
| 8 | (0,67 ‖ 72,0) | − 0.0006 | 3.79 |
| 9 | (65,70 ‖ 71,71) | − 0.0010 | 4.52 |
| 10 | (67,67 ‖ 71,71) | 0.0746 | 5.29 |
| 11 | (65,67 ‖ 71,71) | − 0.0275 | 6.11 |
| 12 | (57,70 ‖ 71,71) | 0.0008 | 6.64 |

Final-state distribution

| State | (0,0 ‖ 0,0) CI coefficient | $|\langle \Psi_F(I)|\Psi_{GS}(N)\rangle|^2(Rel.)$ | $E^F(eV)$ |
|---|---|---|---|
| 0 | < 0.1000 | 100.0 | 0.00 |
| 1 | 0.9107 | 57368.1 | 0.15 |
| 2 | − 0.3484 | 28728.7 | 1.45 |
| 3 | − 0.1284 | 6170.1 | 2.18 |
| 4 | − 0.0022 | 3222.2 | 4.08 |

**(B)**

| State | Wave function (CI vector) |
|---|---|
| 0 | $\langle 0.1000(0,0 ‖ 0,0) + 0.8997(0,70 ‖ 71,0) + 0.2568(67,70 ‖ 71,71)$ <br> $- 0.1158(65,70 ‖ 71,71) + 0.1005(57,70 ‖ 71,71) + \cdots$ |
| 1 | $0.9107(0,0 ‖ 0,0) - 0.2530(0,67 ‖ 71,0) - 0.2518(67,67 ‖ 71,71) + \cdots$ |
| 2 | $- 0.3485(0,0 ‖ 0,0) - 0.7876(0,67 ‖ 71,0) - 0.2913(0,65 ‖ 71,0)$ <br> $- 0.2820(67,67 ‖ 71,71) + \cdots$ |
| 3 | $- 0.1284(0,0 ‖ 0,0) + 0.8344(0,65 ‖ 71,0) + 0.3786(65,67 ‖ 71,71) + \cdots$ |
| 4 | $\langle 0.1000(0,0 ‖ 0,0) + 0.2568(0,67 ‖ 71,0) - 0.2225(0,65 ‖ 71,0)$ <br> $+ 0.2630(0,61 ‖ 71,0) + 0.4724(0,70 ‖ 75,0) - 0.3115(0,67 ‖ 72,0) + \cdots$ |

TABLE XI. Comparison of selected computational and experimental properties of PNA, 2,6-ANN, and 1,4-ANN (energies in eV). The theoretical results were obtained using Nishimoto–Mataga integrals. Comparison of PNA results obtained using the modified oxygen parameters of Jacques *et al.* [$\beta(O) = -30.0$ eV, (Ref. 66)] are included to show that the ground and equivalent-core properties are not greatly modified relative to the original scheme [$\beta(O) = -45.0$ eV]. $\beta$ appears in the off-diagonal Fock matrix elements, and therefore it is expected that going from $\beta(O) = -45.0 \to -30.0$ eV will primarily yield modifications to those orbitals where *both* the oxygen and nitrogen atoms have large coefficients. In accord with this argument the LUMO level is lowered by 0.65 eV, whereas the HOMO level is relatively stable. Note that the PNA results [$\beta(O) = -45.0$ eV] yield a neutral molecule excited state close to the experimental vapor phase value. It should be emphasized that the singly plus doubly excited equivalent-core results were obtained using Pariser–Parr integrals, and thus the singly excited energies given here are not directly comparable to those shown in Tables I, II, VII A, and VIII A. It has been shown in connection with semiempirical methods such as CNDO/S that Pariser–Parr integrals appear better suited to describe systems or configurations which exhibit large correlation effects, whereas Nishimoto–Mataga integrals generally yield better lower-lying closed-shell singlet properties (Refs. 46 and 67–69). The choice of specific parameter options used throughout this work was based on this criterion.

| | PNA | | 2,6-ANN | 1,4-ANN |
|---|---|---|---|---|
| | $\beta(O) = -30.0$ | $\beta(O) = -45.0$ | $\beta(O) = -45.0$ | $\beta(O) = -45.0$ |
| $\epsilon_f^N$(LUMO) | − 3.20 | − 2.55 | − 2.57 | − 2.58 |
| $\epsilon_i^N$(HOMO) | − 10.06 | − 10.00 | − 8.99 | − 8.85 |
| I. P.(EXP) | 8.60[a] | | 8.06[b] | 8.05[b] |
| $^1E_{i\to f}(N)$ | 3.95 | 4.47 | 3.78 | 3.53 |
| $E_{i\to f}^{Z+1}[N1s(NO_2)]$ | 2.78 | 2.77 | 2.38 | 2.59 |
| $^2E_{SU}^{EXP}[N1s(NO_2)]$ | 1.25 | | (?) | (?) |
| $E_{i\to f}^{Z+1}[O1s(NO_2)]$ | 3.32 | 3.32 | 2.45 | 2.92 |
| $^2E_{SU}^{EXP}[O1s(NO_2)]$ | 2.40 | | 1.40 | 1.90 |
| $\langle f(I)|i(N)\rangle[N1s(NO_2)]$ | 0.449 | 0.422 | 0.504 | 0.574 |
| $\langle f(I)|i(N)\rangle[O1s(NO_2)]$ | 0.299 | 0.322 | 0.327 | 0.438 |
| $^1E(N)$–CI | 3.84 | 4.33 | 3.55 | 3.38 |
| $^1E$(EXP) | 3.82(C)[c] | 4.25(V)[d] | 3.40(C)[c] | 3.29(C)[c] |

[a] Experimental values from Ref. 64.
[b] Experimental values from Ref. 5.
[c] Experimental values from Ref. 61.
[d] Experimental values from Ref. 60.

TABLE XII. Bond lengths and bond angles with standard deviations for 2,6-ANN.

| Bond lengths (Å) | | Bond angles (Å) | |
|---|---|---|---|
| O(1)–N(2) | 1.231 (2) | C(2)–N(1)–H(NA) | 116.8 (17) |
| O(2)–N(2) | 1.228 (3) | C(2)–N(1)–H(NB) | 117.9 (18) |
| N(1)–C(2) | 1.371 (4) | H(NA)–N(1)–H(NB) | 125.1 (25) |
| N(1)–H(NA) | 0.87 (2) | O(1)–N(2)–O(2) | 122.2 (2) |
| N(1)–H(NB) | 0.88 (3) | O(1)–N(2)–C(6) | 119.3 (2) |
| N(2)–C(6) | 1.458 (3) | O(2)–N(2)–C(6) | 118.5 (2) |
| C(1)–C(2) | 1.382 (3) | C(2)–C(1)–C(9) | 121.1 (2) |
| C(1)–C(9) | 1.407 (3) | C(2)–C(1)–H(1) | 120.0 (13) |
| C(1)–H(1) | 0.95 (2) | C(9)–C(1)–H(1) | 118.9 (13) |
| C(2)–C(3) | 1.422 (3) | N(1)–C(2)–C(1) | 122.1 (2) |
| C(3)–C(4) | 1.352 (3) | N(1)–C(2)–C(3) | 118.9 (2) |
| C(3)–H(3) | 0.95 (2) | C(1)–C(2)–C(3) | 118.9 (2) |
| C(4)–C(10) | 1.420 (3) | C(2)–C(3)–C(4) | 121.3 (2) |
| C(4)–H(4) | 0.96 (2) | C(2)–C(3)–H(3) | 115.9 (11) |
| C(5)–C(6) | 1.373 (3) | C(4)–C(3)–H(3) | 122.8 (11) |
| C(5)–C(10) | 1.405 (3) | C(3)–C(4)–C(10) | 120.9 (2) |
| C(5)–H(5) | 0.95 (2) | C(3)–C(4)–H(4) | 120.5 (12) |
| C(6)–C(7) | 1.408 (3) | C(10)–C(4)–H(4) | 118.6 (12) |
| C(7)–C(8) | 1.359 (3) | C(6)–C(5)–C(10) | 119.7 (2) |
| C(7)–H(7) | 0.93 (2) | C(6)–C(5)–H(5) | 119.3 (12) |
| C(8)–C(9) | 1.424 (3) | C(10)–C(5)–H(5) | 121.0 (12) |
| C(8)–H(8) | 0.93 (2) | N(2)–C(6)–C(5) | 118.7 (2) |
| C(9)–C(10) | 1.429 (3) | N(2)–C(6)–C(7) | 119.2 (2) |
| | | C(5)–C(6)–C(7) | 122.1 (2) |
| | | C(6)–C(7)–C(8) | 118.8 (2) |
| | | C(6)–C(7)–H(7) | 117.7 (11) |
| | | C(8)–C(7)–H(7) | 123.4 (11) |
| | | C(7)–C(8)–C(9) | 121.7 (2) |
| | | C(7)–C(8)–H(8) | 119.5 (13) |
| | | C(9)–C(8)–H(8) | 118.7 (13) |
| | | C(1)–C(9)–C(8) | 122.6 (2) |
| | | C(1)–C(9)–C(10) | 119.2 (2) |
| | | C(8)–C(9)–C(10) | 118.2 (2) |
| | | C(4)–C(10)–C(5) | 122.1 (2) |
| | | C(4)–C(10)–C(9) | 118.5 (2) |
| | | C(5)–C(10)–C(9) | 119.4 (2) |

$O1s(NO_2)$ solid-state spectrum similar to PNA.[1,2] We have recently found such correspondence in the vapor phase spectra as well.[70] We take these similarities as an experimental indication that hydrogen bonding is not the primary source of the active coupling. Identifying systems with core-hole spectra providing conclusive tests for these concepts continues to be an interesting challenge.

## APPENDIX

The bond lengths and bond angles with standard deviations for 2,6-ANN is given in Table XII.

## ACKNOWLEDGMENT

[1] K. Siegbahn, C. Nordling, A. Fahlman, R. Nordberg, K. Hamrin, J. Hedman, G. Johansson, T. Bergmark, S. E. Karlsson, I. Lindgren, and B. Lindberg, Nova Acta Regiae Soc. Sci. Ups. Ser. IV 20, 1 (1967).

[2] S. Pignataro and G. Distefano, J. Electron. Spectrosc. Relat. Phenom. 2, 171 (1973).

[3] S. Pignataro, R. DiMarino, and G. Distefano, J. Electron. Spectrosc. Relat. Phenom. 4, 90 (1974).

[4] S. Pignataro and G. Distefano, Z. Naturforsch. Teil A 30, 815 (1975).

[5] G. Distefano, D. Jones, A. Modelli, and S. Pignataro, Phys. Scr. 16, 373 (1977).

[6] S. Tsuchiya and M. Seno, Chem. Phys. Lett. 54, 132 (1978).

[7] W. Domcke, L. S. Cederbaum, J. Schirmer, and W. von Niessen, Phys. Rev. Lett. 42, 1237 (1979); Chem. Phys. 39, 149 (1979).

[8] L. S. Cederbaum, W. Domcke, J. Schirmer, and W. von Niessen, Phys. Scr. 21, 481 (1980).

[9] F. P. Colonna, G. Distefano, M. Guerra, and D. Jones, J. Electron. Spectrosc. Relat. Phenom. 18, 309 (1980).

[10] R. Nakagaki, D. C. Frost, and C. A. McDowell, J. Electron. Spectrosc. Relat. Phenom. 19, 355 (1980).

[11] A. Raudino and F. Battaglia, J. Electron. Spectrosc. Relat. Phenom. 20, 327 (1980).

[12] M. S. Banna, Chem. Phys. 45, 383 (1980).

[13] G. Distefano, M. Guerra, D. Jones, A. Modelli, and P. Colonna, Chem. Phys. 52, 389 (1980).

[14] H.-J. Freund and R. W. Bigelow, Chem. Phys. 55, 407 (1981).

[15] R. W. Bigelow and H.-J. Freund, Chem. Phys. Lett. 77, 261 (1981).

[16] R. W. Bigelow, R. J. Weagley, and H.-J. Freund, Chem. Phys. Lett. 82, 305 (1981).

[17] G. Distefano, M. Guerra, D. Jones, and A. Modelli, Chem. Phys. 59, 169 (1981).

[18] A. Katrib and N. R. El-Rayyes, Chem. Phys. 59, 443 (1981).

[19] G. Distefano, M. Guerra, D. Jones, and A. Modelli, Chem. Phys. 68, 383 (1982).

[20] G. Distefano, M. Guerra, F. P. Colonna, D. Jones, G. Consiglio, and D. Spinelli, Chem. Phys. 72, 267 (1982).

[21] P. C. Ford and I. H. Hillier, Chem. Phys. Lett. 92, 141 (1982).

[22] N. J. Fitzpatrick and A. Katrib, J. Electron Spectrosc. Relat. Phenom. 25, 79 (1982).

[23] R. Nakagaki, D. C. Frost, and C. A. McDowell, J. Electron. Spectrosc. Relat. Phenom. 27, 69 (1982).

[24] R. W. Bigelow, R. J. Weagley, and H.-J. Freund, J. Electron. Spectrosc. Relat. Phenom. 28, 149 (1982).

[25] H. Ågren, B. O. Roos, P. S. Bagus, U. Gelius, P. Å. Malmquist, S. Svensson, R. Maripuu, and K. Siegbahn, J. Chem. Phys. 77, 3893 (1982).

[26] M. Guerra, D. Jones, F. P. Colonna, G. Distefano, and A. Modelli, Chem. Phys. Lett. 98, 522 (1983).

[27] A. R. Slaughter, M. S. Banna, and C. A. McDowell, Chem. Phys. Lett. 98, 531 (1983).

[28] P.-Å. Malmquist, S. Svensson, and H. Ågren, Chem. Phys. 76, 429 (1983).

[29] H. Ågren, Int. J. Quantum Chem. 23, 577 (1983).

[30] P. C. Ford and I. H. Hillier, Chem. Phys. 84, 203 (1984).

[31] (a) T. Åberg, Ann. Acad. Sci. Fenn. Ser. A VI, 308, 7 (1969); (b) R. Manne and T. Åberg, Chem. Phys. Lett. 7, 282 (1970).

[32] P. S. Bagus, M. Schrenk, D. W. Davis, and D. A. Shirley, Phys. Rev. A 9, 1090 (1974).

[33] R. L. Martin and D. A. Shirley, J. Chem. Phys. 64, 3685 (1976).

[34] W. R. Salaneck, R. W. Bigelow, H.-J. Freund, and E. W. Plummer, Phys. Rev. B 24, 2403 (1981).

[35] B. P. Tonner, C. M. Kao, E. W. Plummer, T. C. Caves, R. P. Messmer, and W. R. Salaneck, Phys. Rev. Lett. 51, 1378 (1983).

[36] C. J. Nelin, P. S. Bagus, J. Behm, and C. R. Brundle, Chem. Phys. Lett. 105, 58 (1984).

[37] T. D. Thomas and R. W. Shaw, Jr., J. Electron. Spectrosc. Relat. Phenom. 5, 1081 (1974).

[38] M. O. Krause, in *Synchrotron Radiation Research*, edited by H. Winick and S. Doniach (Plenum, New York, 1980).

[39] C. S. Fadley, Ph. D. thesis, Lawrence Berkeley Laboratory, 1970.

[40] A. A. Bakke, H. -W. Chen, and W. L. Jolly, J. Electron. Spectrosc. Relat. Phenom. 20, 333 (1980).

[41] G. M. Sheldrick, SHELX 76 (University of Cambridge, 1976). A program for crystal structure determination.

[42] J. Donohue and K. N. Trueblood, Acta Crystallogr. 9, 960 (1956).

[43] J. E. DelBene and H. H. Jaffé, J. Chem. Phys. 48, 1807, 4050 (1968); 49, 1221 (1968).

[44] R. L. Ellis, G. Kuehnlenz, and H. H. Jaffé, Theor. Chim. Acta 26, 131 (1972).

[45] J. E. DelBene, H. H. Jaffé, R. L. Ellis, and G. Kuehnlenz, QCPE 10, 174 (1974); Program No. 174, Quantum Chemistry Program Exchange, Bloomington, Indiana.

[46] B. Dick and G. Hohlneicher, Theor. Chim. Acta 53, 221 (1979).

[47] (a) R. G. Parr, J. Chem. Phys. 20, 1499 (1952); (b) R. Pariser and R. G. Parr, *ibid.* 21, 767 (1953).

[48] W. L. Jolly and D. N. Hendrickson, J. Am. Chem. Soc. 92, 1863 (1970).

[49] L. J. Aarons, M. F. Guest, and I. H. Hillier, J. Chem. Soc. Faraday Trans. 2 68, 1866 (1972).

[50]P. S. Bagus, M. Schrenk, D. W. Davis, and D. A. Shirley, Phys. Rev. A 9, 1090 (1974).

[51]H. -J. Freund, H. Pulm, B. Dick, and R. Lange, Chem. Phys. 81, 99 (1983).

[52]M. F. Guest, W. R. Rodwell, T. Darko, I. H. Hillier, and J. Kendrick, J. Chem. Phys. 66, 5447 (1977).

[53]W. R. Rodwell, M. F. Guest, T. Darko, I. H. Hillier, and J. Kendrick, Chem. Phys. 22, 467 (1977).

[54]W. H. E. Schwarz, T. C. Chang, and J. P. Connerade, Chem. Phys. Lett. 49, 207 (1977).

[55]R. Arneberg, H. Ågren, P. -Å. Malmquist, and S. Svensson, Chem. Phys. Lett. 92, 125 (1982).

[56]K. Nishimoto and N. Mataga, Z. Phys. Chem. Frankfurt am Main 12, 335 (1957).

[57]J. A. Pople and D. L. Beveridge, *Approximate Molecular Orbital Theory* (McGraw–Hill, New York, 1970), p. 111.

[58]T. Darko, I. H. Hillier, and J. Kendrick, Mol. Phys. 32, 33 (1976).

[59]R. W. Bigelow and H. -J. Freund, J. Chem. Phys. 77, 5552 (1982).

[60]C. C. Teng and A. F. Garito, Phys. Rev. B 28, 6766 (1983).

[61]B. D. Pearson, Tetrahedron 12, 32 (1961).

[62]O. S. Khalil and S. P. McGlynn, J. Lumin. 11, 185 (1975/76).

[63]M. B. Ledger and P. Suppan, Spectrochim. Acta Part A 23, 641 (1967).

[64]O. S. Khalil, J. L. Meeks, and S. P. McGlynn, J. Am. Chem. Soc. 95, 5876 (1973).

[65]T. Veszpremi, Chem. Phys. Lett. 88, 325 (1982).

[66]P. Jacques, J. Faure, O. Chalvet, and H. H. Jaffé, J. Phys. Chem. 85, 473 (1981).

[67]J. Koutecky, J. Chem. Phys. 47, 1501 (1967).

[68]H. M. Chang and H. H. Jaffé, Chem. Phys. Lett. 23, 146 (1973).

[69]H. M. Chang, H. H. Jaffé, and C. A. Masmanidis, J. Phys. Chem. 79, 1118 (1975).

[70]M. S. Banna, A. R. Slaughter, and S. M. Ballina (to be published).